Probabilistic learning of the Purkinje network from the electrocardiogram

Álvarez-Barrientos, Felipe; Salinas-Camus, Mariana; Pezzuto, Simone; Sahli Costabal, Francisco

DOI
10.1016/j.media.2025.103460

Publication date
2025

Document Version
Final published version

Published in
Medical Image Analysis

Citation (APA)
Álvarez-Barrientos, F., Salinas-Camus, M., Pezzuto, S., & Sahli Costabal, F. (2025). Probabilistic learning of the Purkinje network from the electrocardiogram. *Medical Image Analysis*, *101*, Article 103460. https://doi.org/10.1016/j.media.2025.103460

Medical Image Analysis 101 (2025) 103460

Contents lists available at ScienceDirect

Medical Image Analysis

journal homepage: www.elsevier.com/locate/media

Probabilistic learning of the Purkinje network from the electrocardiogram

Felipe Álvarez-Barrientos [a], Mariana Salinas-Camus [b], Simone Pezzuto [c,d], Francisco Sahli Costabal [a,e,f,*]

[a] Department of Mechanical and Metallurgical Engineering, School of Engineering, Pontificia Universidad Católica de Chile, Santiago, Chile
[b] Intelligent Sustainable Prognostics Group, Aerospace Structures and Materials Department, Faculty of Aerospace Engineering, Delft University of Technology, Delft, The Netherlands
[c] Laboratory of Mathematics for Biology and Medicine, Department of Mathematics, Università di Trento, Trento, Italy
[d] Center for Computational Medicine in Cardiology, Euler Institute, Università della Svizzera italiana, Lugano, Switzerland
[e] Institute for Biological and Medical Engineering, Schools of Engineering, Medicine and Biological Sciences, Pontificia Universidad Católica de Chile, Santiago, Chile
[f] Millennium Institute for Intelligent Healthcare Engineering, iHEALTH, Chile

ARTICLE INFO

Dataset link: http://github.com/fsahli/purkinje-learning

Keywords:
Purkinje network
Machine learning
Bayesian inference
Approximate bayesian computation
Digital twin
Cardiac electrophysiology

ABSTRACT

The identification of the Purkinje conduction system in the heart is a challenging task, yet essential for a correct definition of cardiac digital twins for precision cardiology. Here, we propose a probabilistic approach for identifying the Purkinje network from non-invasive clinical data such as the standard electrocardiogram (ECG). We use cardiac imaging to build an anatomically accurate model of the ventricles; we algorithmically generate a rule-based Purkinje network tailored to the anatomy; we simulate physiological electrocardiograms with a fast model; we identify the geometrical and electrical parameters of the Purkinje-ECG model with Bayesian optimization and approximate Bayesian computation. The proposed approach is inherently probabilistic and generates a population of plausible Purkinje networks, all fitting the ECG within a given tolerance. In this way, we can estimate the uncertainty of the parameters, thus providing reliable predictions. We test our methodology in physiological and pathological scenarios, showing that we are able to accurately recover the ECG with our model. We propagate the uncertainty in the Purkinje network parameters in a simulation of conduction system pacing therapy. Our methodology is a step forward in creation of digital twins from non-invasive data in precision medicine. An open source implementation can be found at http://github.com/fsahli/purkinje-learning.

1. Motivation

Cardiovascular diseases are the leading causes of death in the world, taking around 19 million lives in 2020 (Tsao et al., 2023). Arrhythmias, which are abnormal heart rhythms, can lead to the impairment of cardiac function. One of the main components of the cardiac electrical system is the Purkinje network, located in the subendocardium of the ventricles (Vigmond and Stuyvers, 2016). Purkinje cells are larger than cardiomyocytes and have fewer myofibrils and more mitochondria. The electrical propagation of the excitation wave in Purkinje cells is faster than in other cardiac myocytes. A functional Purkinje network is essential to synchronize the activations and contractions of the left and right ventricles and maintain a consistent cardiac rhythm (Dubin, 1996). Purkinje fibers were first documented more than a century ago (Tawara, 1906); yet, to date, there is no technique to fully reconstruct their geometry *in vivo* in humans (Çetingül et al., 2011; Magat et al., 2021; Goodyer et al., 2022; Tsao et al., 2023). Due to these limitations, there have been multiple attempts to represent the Purkinje network with simplified models from a functional and geometric perspective.

From a modeling point of view, the Purkinje network is oftentimes surrogated by a fast-conducting subendocardial layer with a limited number of discrete early activation sites (Pezzuto et al., 2017). Thanks to its small number of parameters, the surrogate model is computationally efficient and enables fast model personalization from clinical data (Giffard-Roisin et al., 2017; Camps et al., 2021; Pezzuto et al., 2021; Gillette et al., 2021b; Grandits et al., 2023). However, the fast-conducting subendocardial layer cannot capture the complexity of the ventricular activation under pathological conditions such as a bundle branch block. Recently, algorithms based on fractal trees (Lindenmayer, 1968) have emerged as a tool for automatic network generation. Current models consist of curved branches that grow on the endocardial surface (Ijiri et al., 2008; Sahli Costabal et al., 2016; Gillette et al.,

* Correspondence to: Vicuña Mackenna 4860, Macul, Santiago, Chile.
E-mail address: fsc@ing.puc.cl (F. Sahli Costabal).

https://doi.org/10.1016/j.media.2025.103460
Received 12 January 2024; Received in revised form 26 December 2024; Accepted 7 January 2025
Available online 21 January 2025

2021a). Other models are generated with hierarchical networks that sub-sequentially add smaller fibers (Sebastian et al., 2011, 2013) or are based on optimization procedures (Berg et al., 2023).

Regardless of the representation, there is an increasing interest in creating a digital twin of the Purkinje network from available clinical data. Considering the lack of imaging modalities available for the Purkinje network, there have been attempts to recover the structure of the Purkinje network from electrical measurements. Early studies focused on invasive electroanatomical mapping data, where activation times inside the ventricles are known (Palamara et al., 2014; Vergara et al., 2014; Cárdenes et al., 2015; Barber et al., 2021). However, in order not to depend on invasive procedures, some approaches base the recovery of the Purkinje network on surface electrocardiograms (ECGs). A common workflow is to first fit the QRS complex of the ECG by optimizing a set of parameters, such as conduction velocity and position and timing of excitation sources, and then use such sources to grow a Purkinje network that can faithfully reproduces the endocardial activation, and thus the ECG (Kahlmann et al., 2017; Gillette et al., 2021a; Camps et al., 2024). The generation of the network, constrained to the endocardial sources, can be based on Prim's and Dijkstra's algorithms (Kahlmann et al., 2017), or obtained by first connecting the sources with major branches, and then growing the rest of the network with a rule-based approach (Gillette et al., 2021a; Camps et al., 2024).

In general, Purkinje network identification from the ECG is a severely ill-posed inverse problem. First, the number of parameters describing the network is high, with several of them only marginally affecting the ECG. Thus, the set of plausible Purkinje networks explaining a given ECG is large. Second, depending on the condition of the patient, parts of the Purkinje network may be blocked and not influence the ventricular activation at all. Here, identification of the tree structure from the ECG is not possible. From a clinical perspective, however, partially blocked parts may be the target of therapeutic options, for instance, conduction system pacing (Ellenbogen et al., 2023). For these reasons, it is fundamental to quantify what is and what is not possible to infer the Purkinje network from the standard ECG.

This work addresses the Purkinje network identification problem with a probabilistic approach. In other words, we aim to recover a *distribution* of Purkinje networks that can explain the observed ECG rather than providing a single estimate. Within a probabilistic framework, we can quantify the uncertainty in the estimation process and assess predictions with confidence intervals. We tackle this challenging problem by integrating advanced techniques that include electrophysiology modeling, machine learning, and probability density estimation. Fig. 1 illustrates the first part of the process. We start by creating a parametric representation of the Purkinje network using fractal trees (Sahli Costabal et al., 2016). Then, we couple the Purkinje network with the myocardium to simulate the ECG using a fast solver based on the eikonal equation (Pezzuto et al., 2017). We find the network parameters that best represent the patient's ECG by defining a loss function that compares the predicted ECG by our model and the observed data (Pezzuto et al., 2021, 2022). We minimize the loss function using Bayesian optimization, a machine-learning technique where the objective function is approximated by a Gaussian process (Garnett, 2023). Once we have a set of parameters that best fits the data, we estimate the distribution of parameters that explain the data by using the Gaussian process of the loss function as a prior distribution for approximate Bayesian computation (Sunnåker et al., 2013). Therefore, we can draw samples from the posterior distribution of parameters.

This manuscript is organized as follows: in Section 2 we present the methodology to generate the Purkinje network, the forward model to compute the ECG for a given Purkinje network, and the probabilistic pipeline to identify a distribution of trees. In Section 3, we show the results of the proposed method in a synthetic example and on 4 patients with different conditions. We finalize this Section by showing the predictive capabilities with quantified uncertainty of our method. We finish this manuscript with a discussion and outlook in Section 4.

2. Methods

2.1. Purkinje network generation

We model the Purkinje network as fractal tree, in a similar way to our previous work (Sahli Costabal et al., 2016). To replicate the physiological structure of the Purkinje network, we select a root node and initial direction and length l_{i} to represent the bundles. Then, we create an arbitrary number of fascicles, which are present in the cardiac conduction system, with different branching angles $\alpha_{\text{F}i}$ and lengths $l_{\text{F}i}$. From the end of each fascicle we start growing the fractal tree. The branches are characterized by 3 parameters that are common for the entire tree: the branch length l_{b}, the branching angle α_{b} and the repulsion parameter w. Each branch is discretized a number of segments N_s which are added simultaneously to end of each growing branch according to the following rule:

$$\boldsymbol{d}^{i+1} = \frac{\boldsymbol{d}^i + w\nabla d_{\text{CP}}(\boldsymbol{x}^i)}{\|\boldsymbol{d}^i + w\nabla d_{\text{CP}}(\boldsymbol{x}^i)\|}, \quad i > 1, \tag{1}$$

$$\boldsymbol{x}^{i+1} = \boldsymbol{x}^i + \frac{l_{\text{b}}}{N_s}\boldsymbol{d}^{i+1}, \tag{2}$$

where $\boldsymbol{d}^{i+1}$ represents the normalized direction of the $(i+1)$-th segment, which is comprised of end point $\boldsymbol{x}^i$, $\boldsymbol{x}^{i+1}$. The function $d_{\text{CP}}(\boldsymbol{x})$ represents the distance to the closest point already in the tree. Thus, the gradient ∇d_{CP} provides a repulsive direction from the existing points. The initial direction $\boldsymbol{d}^1$ of each branch is determined by a rotation of either $+\alpha_{\text{b}}$ or $-\alpha_{\text{b}}$ with respect to the direction of the last segment from the parent branch. The main geometric parameters of the Purkinje tree are shown in Fig. 2, top row.

To avoid the constant projection of new points to the 3D surface, we flatten the ventricular geometry. In particular, we map the endocardial surface with coordinates $\boldsymbol{x} \in \mathbb{R}^3$ to a unit disk with coordinates $\boldsymbol{u} \in \mathbb{R}^2$ using harmonic maps (Remacle et al., 2010), as shown in Fig. 2, bottom row. These maps are quasi-conformal, meaning that angles are approximately preserved. Then, if we draw a straight line in the unit disk, it should remain a straight line in the ventricular geometry. The area is not preserved and we need take into account a scaling factor $s(\boldsymbol{u})$ for the length, such that $\|d\boldsymbol{x}\| = s(\boldsymbol{u})\|d\boldsymbol{u}\|$. To compute the harmonic map, we only need to solve the Laplace equation twice on the surface, which we achieve using finite elements. In particular, we solve the following equations for $\boldsymbol{u} = [u, v]$:

$$\begin{cases} \Delta u = 0 & \boldsymbol{x} \in S^{\text{endo}} \\ u(\boldsymbol{x}) = \sin(2\pi\ell(\boldsymbol{x})/L) & \boldsymbol{x} \in \partial S^{\text{endo}} \\ \Delta v = 0 & \boldsymbol{x} \in S^{\text{endo}} \\ v(\boldsymbol{x}) = \cos(2\pi\ell(\boldsymbol{x})/L) & \boldsymbol{x} \in \partial S^{\text{endo}} \end{cases} \tag{3}$$

where S^{endo} is the endocardial surface, ∂S^{endo} its boundary (the ring at the base), $\ell(\boldsymbol{x})$ is the curvilinear coordinate along the ring from an arbitrary point to $\boldsymbol{x}$, and L is the total length of the ring. We compute the scaling factor $s(\boldsymbol{x})$ as the average of the eigenvalues of the metric $\boldsymbol{G}(\boldsymbol{x}) = \nabla\boldsymbol{u}^T \cdot \nabla\boldsymbol{u}$. For an exact harmonic map, both eigenvalues should be equal, but for a quasi-conformal map, such as the one used here, they should be close, which is the reason why we take the average of them. We note that we cut the endocardial surface for both ventricles with a plane below the valves and arteries to have a single boundary. This is a requirement and a limitation of this approach, but it did not produce any issues for the ventricles. Finally, we remark that the final tree never self-intersects; some terminal points might arrive very close to another branch in a geometrical sense, but topologically, they are never connected.

2.2. Forward ECG model

We model cardiac activation in the Purkinje tree and in the myocardium with the eikonal equation (Pezzuto et al., 2017). The eikonal

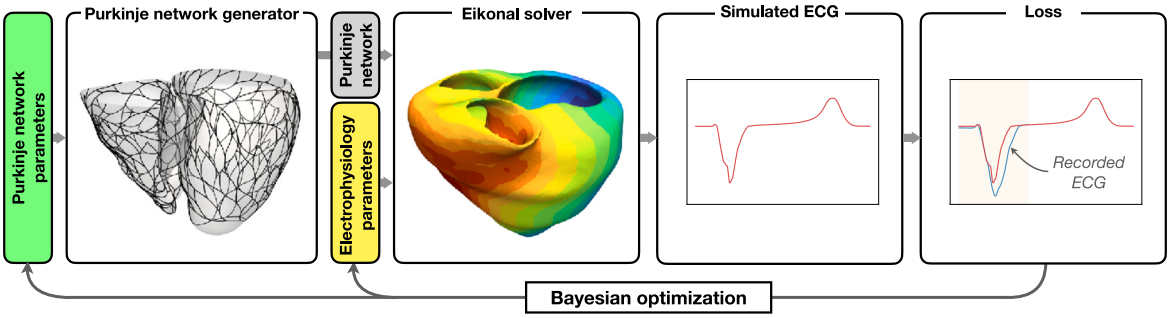

Fig. 1. Process outline. We first create a parametric Purkinje network on the left and right ventricles. For a given Purkinje network and electrophysiology parameters we simulate activation times with the Eikonal equation, from which we can compute an ECG. We compare this ECG with the patient data and attempt to find the optimal parameters with Bayesian optimization.

equation models the spread of the activation front given a (possibly anisotropic) conduction velocity and initiation sites. For the sake of simplicity, we introduce the forward model and the notation for a single Purkinje tree. Here, we denote a Purkinje tree by $\mathcal{P} = \bigcup_{k=1}^{N} \Gamma_k$, where each branch Γ_k is a smooth open curve in $\mathbb{R}^3$. The boundary $\partial\mathcal{P} = \{\boldsymbol{p}_i\}_{i=0}^{M}$ contains the nodes of the tree, denoted by $\boldsymbol{p}_i$. We assume that the nodes are ordered as follows: $\boldsymbol{p}_0$ is the root node; for $i = 1, \dots, M_t$, $\boldsymbol{p}_i$ is a terminal node or Purkinje-Myocardium Junctions (PMJs); for $i = M_t + 1, \dots, M$, $\boldsymbol{p}_i$ is a branching point, that is the intersection of exactly 3 different branches. We represent the active myocardium by a smooth domain $\Omega \subset \mathbb{R}^3$. The PMJs are by definition the points of contact between the Purkinje tree and the myocardium, and specifically the endocardium. That is, $\boldsymbol{p}_i \in \partial\Omega$, $i = 1, \dots, M_t$.

The activation in the tree, denoted by $\tau^{\mathcal{P}} : \bar{\mathcal{P}} \to \mathbb{R}$, measures the travel time from the root node to the rest of the tree. Similarly, $\tau^{\mathcal{M}} : \Omega \to \mathbb{R}$ is the activation map in the myocardium. They solve the following systems:

$$\begin{cases} c^{\mathcal{P}}(\boldsymbol{x})|\nabla\tau^{\mathcal{P}}(\boldsymbol{x}) \cdot \boldsymbol{t}(\boldsymbol{x})| = 1, & \boldsymbol{x} \in \mathcal{P}, \\ \tau^{\mathcal{P}}(\boldsymbol{p}_0) = t_0, & \\ \tau^{\mathcal{P}}(\boldsymbol{p}_i) = \min\{\tau^{\mathcal{M}}(\boldsymbol{p}_i), \tau^{\mathcal{P}}(\boldsymbol{p}_i)\}, & \boldsymbol{p}_i \in \partial P, i = 1, \dots, M_t, \\ \tau^{\mathcal{P}}(\boldsymbol{p}_i) = \min\{\tau^{\mathcal{P}}|_{\partial\mathcal{P}}(\boldsymbol{p}_i)\}, & i = M_t + 1, \dots, M, \end{cases} \tag{4}$$

for the Purkinje activation, where $c^{\mathcal{P}} : \mathcal{P} \to \mathbb{R}$ and $\boldsymbol{t}$ are respectively the conductivity velocity field and the tangent field in the Purkinje tree. The first term is the eikonal equation in the tree, the second term is

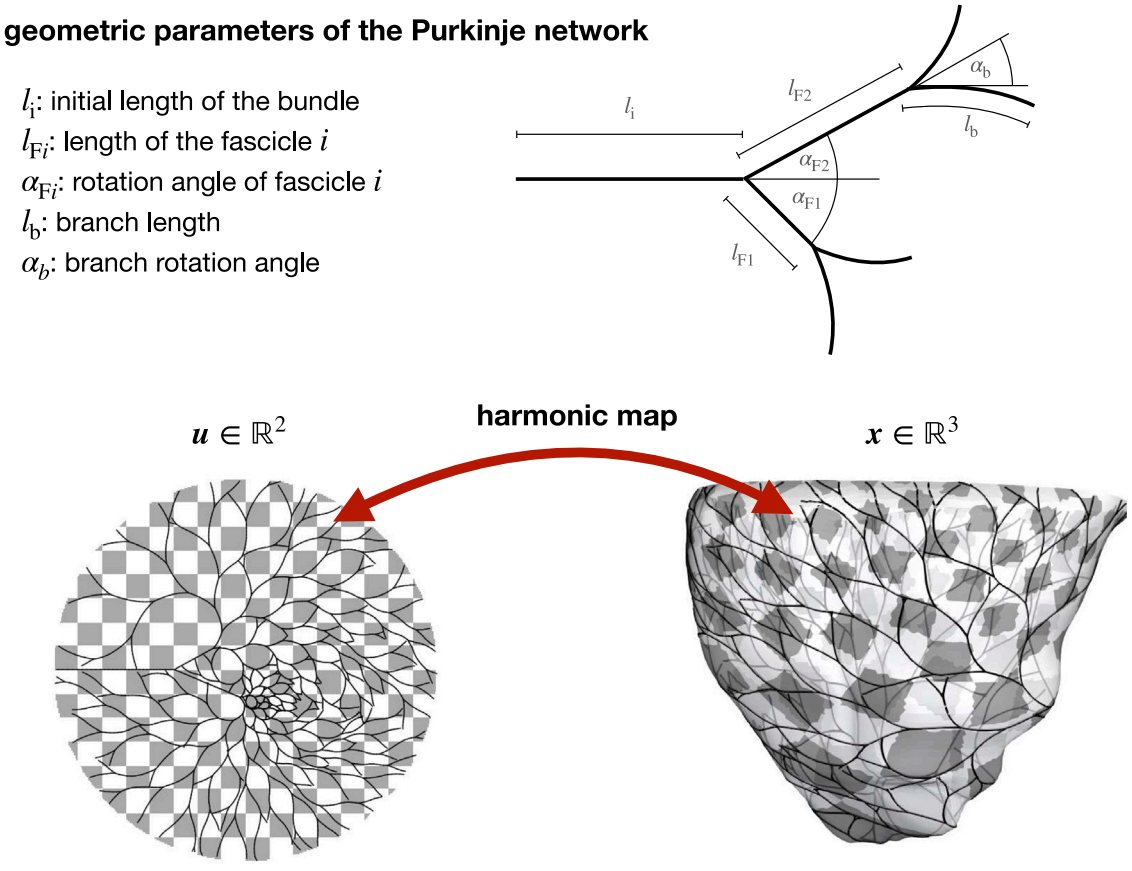

Fig. 2. Purkinje network generation. Top, we show the geometric parameters that determine the structure of the Purkinje network. Bottom, we use a harmonic map to grow the Purkinje network in 2D, which is later mapped to the endocardial surface.

the boundary condition at the root point. The third term represents that coupling between the Purkinje tree and the myocardium at the PMJs and considers a potential activation from the myocardium to the tree. The last term is the connection between branches of the tree. For the myocardium, we have

$$\begin{cases} \sqrt{\left(\boldsymbol{D}(\boldsymbol{x})\nabla\tau^{\mathcal{M}}(\boldsymbol{x})\cdot\nabla\tau^{\mathcal{M}}(\boldsymbol{x})\right)} = 1, & \boldsymbol{x}\in\Omega, \\ \tau^{\mathcal{M}}(\boldsymbol{p}_i) = \min\left\{\tau^{\mathcal{M}}(\boldsymbol{p}_i), \tau^{\mathcal{P}}(\boldsymbol{p}_i)\right\}, & \boldsymbol{p}_i\in\partial P, i=1,\dots,M_t, \end{cases} \tag{5}$$

where $\boldsymbol{D}^{\mathcal{M}}:\Omega\to\mathbb{R}^{3\times3}$ is the conductivity tensor field, assumed symmetric, positive-definite. In the myocardium, the tensor $\boldsymbol{D}$ is linked to the electric conductivity of the monodomain equation as follows (Pezzuto et al., 2017)

$$\boldsymbol{D}(\boldsymbol{x}) = \alpha^2\boldsymbol{G}_i(\boldsymbol{G}_i+\boldsymbol{G}_e)^{-1}\boldsymbol{G}_e, \tag{6}$$

$$\boldsymbol{G}_{\{i,e\}} = \sigma_t^{\{i,e\}}\mathbf{I} + \left(\sigma_l^{\{i,e\}} - \sigma_t^{\{i,e\}}\right)\boldsymbol{f}(\boldsymbol{x})\otimes\boldsymbol{f}(\boldsymbol{x}), \tag{7}$$

where $\boldsymbol{G}_i$ and $\boldsymbol{G}_e$ respectively the intracellular and extracellular conductivity tensor, α is a scaling constant, $\boldsymbol{f}(\boldsymbol{x})$ is the fiber field, and $\sigma_{\{l,t\}}^{\{i,e\}}$ are the intra-/extra-cellular conductivities longitudinal and orthogonal to the fibers.

Note that in (4) the activation map at a branching point, $\tau^{\mathcal{P}}|_{\partial\mathcal{P}}(\boldsymbol{p}_i)$, is multi-valued, because multiple branches contribute to the same point. In the last equation of (4) we enforce the solution at $\boldsymbol{p}_i$ to the minimum across all terminal points of incoming branches. The equations have a simple interpretation: within each branch or in the myocardium, $\tau(\boldsymbol{x})^{\mathcal{P}}$ and $\tau(\boldsymbol{x})^{\mathcal{M}}$ solve the eikonal equation. The activation at the PMJs is the earliest between those arriving either from the tree or from the myocardium. In other words, the coupling is bidirectional: either the electric signal from the tree activates the myocardium (orthodromic or normal activation), or the electric signals enters into the tree from the myocardium (antidromic activation). Note that we do not consider here activation delays at the PMJs, as it normally would happen due to a source–sink mismatch (Vigmond and Stuyvers, 2016).

The coupled problem (4)–(5) is well-posed and has a unique viscosity solution for every choice of the initial root time t_0. To see this, we note that the solution in the myocardium can be written as:

$$\tau^{\mathcal{M}}(\boldsymbol{x}) = \min_{i=1,\dots,M_t}\left\{\delta^{\mathcal{M}}(\boldsymbol{p}_i,\boldsymbol{x}) + \tau^{\mathcal{P}}(\boldsymbol{p}_i)\right\}, \tag{8}$$

where $\delta^{\mathcal{M}}(\boldsymbol{y},\boldsymbol{x})$ is the travel time along the geodesic path in $\bar{\Omega}$ connecting $\boldsymbol{x}$ and $\boldsymbol{y}$. Similarly,

$$\tau^{\mathcal{P}}(\boldsymbol{x}) = \min\left\{\delta^{\mathcal{P}}(\boldsymbol{p}_0,\boldsymbol{x}) + t_0, \min_{i=1,\dots,M_t}\left\{\delta^{\mathcal{P}}(\boldsymbol{p}_i,\boldsymbol{x}) + \tau^{\mathcal{M}}(\boldsymbol{p}_i)\right\}\right\}, \tag{9}$$

where $\delta^{\mathcal{P}}(\boldsymbol{y},\boldsymbol{x})$ is the travel time in the Purkinje tree $\bar{\mathcal{P}}$.

The numerical algorithm for solving the coupled problem (4)–(5) is inspired by the above formula. Given $\tau_0^{\mathcal{M}}(\boldsymbol{x}) = +\infty$ we iterate, for $n\geq0$,

$$\begin{cases} \tau_{n+1}^{\mathcal{P}}(\boldsymbol{x}) = \min\left\{\delta^{\mathcal{P}}(\boldsymbol{p}_0,\boldsymbol{x}) + t_0, \min_{i=1,\dots,M_t}\left\{\delta^{\mathcal{P}}(\boldsymbol{p}_i,\boldsymbol{x}) + \tau_n^{\mathcal{M}}(\boldsymbol{p}_i)\right\}\right\}, \\ \tau_{n+1}^{\mathcal{M}}(\boldsymbol{x}) = \min_{i=1,\dots,M_t}\left\{\delta^{\mathcal{M}}(\boldsymbol{p}_i,\boldsymbol{x}) + \tau_{n+1}^{\mathcal{P}}(\boldsymbol{p}_i)\right\}. \end{cases} \tag{10}$$

The algorithm readily generalizes to the case of two independent Purkinje trees for the left and right ventricle. We note that the myocardium may couple the trees: for instance, the right activation may occur much earlier than the left activation, thus myocardial activation in the left ventricle will enter into the left Purkinje tree and overshadow the intrinsic activation. This is the case of a left bundle branch block.

For the discretization in space, we consider a piecewise linear approximation $\mathcal{P}_h$ for $\mathcal{P}$ and a general conformal mesh Ω_h of Ω. We approximate the conduction velocity as a piecewise-constant function on the elements of the mesh. The numerical solution of the eikonal equation on the Purkinje tree $\mathcal{P}_h$ and in the myocardium is based on the Fast Iterative Method (Fu et al., 2013), implemented on GPU (Pezzuto et al., 2017). For the coupling, the PMJs are not necessarily vertices of the myocardial mesh. In this way, we can avoid remeshing of the myocardial mesh or constraining the PMJs during the tree generation. Hence, we apply the following boundary conditions:

$$\tau^{\mathcal{M}}(\mathbf{x}_j) = \sqrt{\left(\boldsymbol{D}^{-1}(\boldsymbol{p}_i)(\boldsymbol{x}_j-\boldsymbol{p}_i)\cdot(\boldsymbol{x}_j-\boldsymbol{p}_i)\right)} + \tau^{\mathcal{P}}(\boldsymbol{p}_i), \tag{11}$$

where $\mathbf{x}_j$ are the nodes of the element containing $\mathbf{p}_i$. That is, we solve exactly the eikonal equation within the element.

The surface ECG is computed via the lead field approach (Pezzuto et al., 2017; Potse, 2018). Given the lead fields $Z_\ell(\boldsymbol{x}):\Omega\to\mathbb{R}$, for $\ell=1,\dots,12$, the ℓ-lead of the surface ECG is as follows:

$$V_\ell(t) = \int_\Omega \mathbf{G}_i(\boldsymbol{x})\nabla U\left(t-\tau^{\mathcal{M}}(\boldsymbol{x})\right)\cdot\nabla Z_\ell(\boldsymbol{x})\,\mathrm{d}\boldsymbol{x}, \tag{12}$$

where $U(\xi)$ is a template action potential. In this work, $U(\xi)$ has been computed from a 1D cable simulation with the Ten Tusscher–Panfilov model (ten Tusscher et al., 2004). We neglect the contribution of the Purkinje tree on the ECG. The lead fields $Z_\ell(\boldsymbol{x})$ are computed once in the torso domain by solving the bidomain equation (Potse, 2018).

2.3. Purkinje network estimation

Using the Purkinje network generation algorithm and the forward ECG model, we expect to find possible representations of the Purkinje tree for a specific patient. For each case, we have the 12-lead ECG time series, that we call reference ECG $\hat{\mathbf{V}}(t)$. Then the task is to find possible trees for the patient Purkinje network, such that the generated ECG $\mathbf{V}(t;\boldsymbol{\theta})$ matches the data $\hat{\mathbf{V}}(t)$ in a least-squares sense. We note that the generated ECG $\mathbf{V}(t;\boldsymbol{\theta})$ depends on geometric and electrophysiology parameters of the Purkinje network, which we summarize in a vector $\boldsymbol{\theta}$. As geometric parameters, we choose the left and right initial length l_{i}^{L}, l_{i}^{R}; and 2 fascicles lengths and fascicles angles for each ventricle $l_{\mathrm{Fi}}^{\mathrm{L}}$, $l_{\mathrm{Fi}}^{\mathrm{R}}$, $\alpha_{\mathrm{Fi}}^{\mathrm{L}}$, $\alpha_{\mathrm{Fi}}^{\mathrm{R}}$ with $i\in\{1,2\}$. We fix the remaining geometric parameters, selecting a branch length l_{b} of 8 mm, the number of segments N_s to 8, the repulsion parameter w to 0.1, a branch angle α_{b} to 0.15 rad, and 20 branch generations (Sahli Costabal et al., 2016). A sensitivity study showed that accurate reconstructions were possible even if these parameters where fixed, thus reducing the dimensionality of the problem. For electrophysiology parameters, we choose the conduction velocity of the Purkinje network and the delay between the activation of the left and right ventricle, which we call "root time". If this parameter is positive, it means that the right Purkinje tree activated later than the left, and vice versa. Considering both geometric and electrophysiology parameters, we need to estimate 12 parameters, thus $\boldsymbol{\theta}\in\mathbb{R}^{12}$. We define a plausible range for the parameters for the search, shown in Table 1.

Thus, we have to find the parameters $\boldsymbol{\theta}_{\min}$ that minimize the difference between $\hat{\mathbf{V}}(t)$ and $\mathbf{V}(t;\boldsymbol{\theta})$. We compute the mismatch by taking into the account only the QRS complex of the ECGs, which corresponds to the ventricular activation. Further details on the pre-processing of the ECG are given in Section 2.6. The QRS onset of the simulated ECG may also vary, because the Purkinje networks vary and also because the Q deflection, which corresponds to the first epicardial breakthrough, is usually 10–15 ms late with respect to endocardial activation. Therefore, we use cross-correlation to find the best alignment between the signals. Then, as an optimization objective, we select the L^2 norm of the difference between the QRS complexes:

$$y(\boldsymbol{\theta}) = \frac{1}{T}\int_0^T\left(\hat{\mathbf{V}}(t)-\mathbf{V}(t;\boldsymbol{\theta})\right)^2\mathrm{d}t, \tag{13}$$

where T is the QRS duration. We remark that our approach can work with alternative choices of the ECG metric (13) (Grandits et al., 2022).

Finally, we aim to solve the following parameter estimation problem:

$$\boldsymbol{\theta}_{\min} = \arg\min_{\boldsymbol{\theta}} y(\boldsymbol{\theta}). \tag{14}$$

The summary of the steps is shown in Fig. 1. We use Bayesian optimization for solving (14).

Table 1
Geometric and electrophysiology parameters, with their symbols. The table shows the search range of the parameters to be found and a single value for the fixed parameters. The $(\cdot)^L$ and $(\cdot)^R$ indicate the left and right ventricle parameters, respectively.

	Parameter	Symbol	Range/Value
Geometric parameters	Initial length	l_i^L, l_i^R	30 to 100 mm
	Fascicles lengths	l_{F1}^L, l_{F2}^L, l_{F1}^R, l_{F2}^R	2 to 50 mm
	Fascicles angles	α_{F1}^L, α_{F2}^L, α_{F1}^R, α_{F2}^R	$-\pi/4$ to $3\pi/4$ rad
	Branch length	l_b	8 mm
	Branching angle	α_b	0.15 rad
	Repulsion parameter	w	0.1
	Number of segments	N_s	8
	Number of generations	N_{it}	20
Electrophysiology parameters	Root time	RT	−75 to 50 ms
	Conduction velocity	CV	2 to 4 m/s
	Conduction velocity in myocardium	CV_{myo}	0.8 m/s

2.4. Bayesian optimization

Bayesian optimization is an approach to efficiently minimize complex and costly functions, used in areas such as machine learning, physical systems, and field experiments (Blanchard and Sapsis, 2021; Garnett, 2023). This approach combines principles of Bayesian inference and optimization, to find a global optimal solution while minimizing the number of data required. There are two main aspects of the Bayesian optimization. The first one is the surrogate model, which approximates the objective function given known data points. The surrogate model should be faster to evaluate than the original model and it should also provide uncertainty estimates.. The second is the acquisition function, which selects new points in the parameter space by balancing the exploration of regions with high uncertainty and the exploitation of areas with low objective function.

In our application, for each patient, we begin by training a surrogate model with N previously computed points $\{\boldsymbol{\Theta}, \boldsymbol{y}\} = \{(\theta_i, y_i)_{i=1}^N\}$, where y_i represents the mismatch between measured and generated ECGs, defined in Eq. (13), and θ_i represents the parameters of the Purkinje network, as previously described. Then, we construct our surrogate model by representing the relationship between $\boldsymbol{\theta}$ and $\boldsymbol{y}$ as

$$\boldsymbol{y} = f(\boldsymbol{\theta}) + \varepsilon, \tag{15}$$

where f is the latent function we want to infer and ε is a noise that may corrupt the output. For simplicity, we assume ε as Gaussian and uncorrelated, $\varepsilon \sim \mathcal{N}(\mathbf{0}, \sigma_n^2 \boldsymbol{I})$, where σ_n^2 is an unknown variance parameter that will be learned from the data. In the case where the relationship between $\boldsymbol{\theta}$ and $\boldsymbol{y}$ is noiseless (i.e. deterministic), a small level of noise is still considered for numerical reasons. For the latent function f we assume a zero-mean Gaussian process prior

$$f(\boldsymbol{\theta}) \sim \mathcal{GP}\big(\mathbf{0}, k(\boldsymbol{\theta}, \boldsymbol{\theta}'; \boldsymbol{\beta})\big), \tag{16}$$

where $k(\boldsymbol{\theta}, \boldsymbol{\theta}'; \boldsymbol{\beta})$ is the covariance kernel function, which represents our knowledge about the objective function behavior and depends on a set of hyper-parameters $\boldsymbol{\beta}$. In each step of the optimization, with the known data $\{\boldsymbol{\Theta}, \boldsymbol{y}\}$ we train the model with the end of finding the hyper-parameters $\boldsymbol{\beta}$ that explain their underlying relationship. Here we adopt the Automatic Relevance Determination (ARD) exponential kernel (Despotovic et al., 2020; Kumar et al., 2021)

$$k(\boldsymbol{\theta}, \boldsymbol{\theta}'; \boldsymbol{\beta}) = \eta^2 \cdot \exp(-r), \tag{17}$$

where $\boldsymbol{\beta} = \{\eta, r_1, \ldots, r_n\}$, with η the signal standard deviation and

$$r = \sqrt{\sum_{i=1}^{n} \frac{(\theta_i - \theta_i')^2}{r_i^2}}, \tag{18}$$

where r_i is the length scale of the kernel function in the input dimension i, so with increasing r_i the influence of the ith input decreases. Once the model is trained we can obtain the posterior mean $\mu(\boldsymbol{\theta})$ and variance $\sigma^2(\boldsymbol{\theta})$ at any point, which represent the predicted value of our surrogate model and its uncertainty, respectively (Rasmussen and Williams, 2006). With this information we make use of the acquisition function to determine $\boldsymbol{\theta}_{N+1}$, the next point to acquire and incorporate to our dataset. This function varies in the parameter space and depends on value of the prediction and its uncertainty, such that $a(\mu(\boldsymbol{\theta}), \sigma^2(\boldsymbol{\theta}))$. The acquisition function maximizes improvement by considering both the expected function value, and the level of certainty on the prediction, at each point. This allows optimization method to balance exploration and exploitation. Then, to select the next point where to acquire the data, we solve the following optimization problem:

$$\boldsymbol{\theta}^{N+1} = \arg\max_{\boldsymbol{\theta}} a(\mu(\boldsymbol{\theta}), \sigma^2(\boldsymbol{\theta})) \tag{19}$$

There are many options of acquisition functions, here we select expected improvement (Jones et al., 1998), one of the most widely-used in Bayesian optimization. Then, we find $\boldsymbol{\theta}^{N+1}$ using the minimize function from the SciPy library (Virtanen et al., 2020), with the L-BFGS-B algorithm and restarting the optimization 50 times with different initial guesses, to finally select the best solution. Every acquisition requires the solution of the forward ECG model to obtain the new pair $(\boldsymbol{\theta}_{N+1}, y_{N+1})$. For each simulation presented in this work, first we use the forward ECG model to sample 250 points with Latin hypercube sampling, and then we perform the Bayesian optimization for 300 steps.

2.5. Posterior distribution estimation

After the optimization, the goal is to estimate the posterior distribution of the Purkinje network parameters. For this task, we use Approximate Bayesian Computation (ABC) (Sunnåker et al., 2013). ABC is a likelihood-free inference technique that only requires defining a prior distribution and a distance function. Algorithmically, this method is straightforward: it generates a sample from the prior distribution and it accepts it if the distance between the measurements and the simulated data is less than a given tolerance. This process is repeated until sufficient samples are accumulated. We take advantage of trained Gaussian process surrogate for the Bayesian optimization to create an informed prior distribution. We note that this is not a prior in the pure Bayesian sense, which represents the beliefs on $\boldsymbol{\theta}$ before observing the data, but it is still useful. Here, samples with a low predicted value of the loss function will be assigned a higher probability to enter the posterior distribution. We also take into account the predicted uncertainty of the Gaussian process and assign less prior probability to points with high predicted variance. With these two considerations, we define the prior probability density as:

$$p(\boldsymbol{\theta}) = \frac{1}{\sqrt{2\pi\left(\sigma^2(\boldsymbol{\theta}) + \sigma_{\min}^2\right)}} \exp\left(-\frac{1}{2}\frac{(\mu(\boldsymbol{\theta}) - y_{\min})^2}{\left(\sigma^2(\boldsymbol{\theta}) + \sigma_{\min}^2\right)}\right) \tag{20}$$

where $y_{\min}$ and $\sigma_{\min}^2$ correspond to the mean and variance prediction of the Gaussian point at the point $\boldsymbol{\theta}_{\min}$ found during the optimization. We expect that $p(\boldsymbol{\theta})$ will be maximized at $\theta_{\min}$, as is unlikely that the Gaussian process will predict any lower values than the optimum found after the 300 rounds of optimization. We note that even though the prior distribution resembles a Gaussian, it is not possible directly sample $\boldsymbol{\theta}$ from its definition, as the mean and variance depend on $\boldsymbol{\theta}$ through a Gaussian process. Thus, we rely on rejection sampling (Robert and Casella, 2013), a well-known algorithm to obtain samples from a target distribution. To obtain samples from the prior distribution, we generate $N_s = 5.000.000$ uniformly distributed random samples of $\boldsymbol{\theta}$. For each point, we use the Gaussian process previously trained (with the 250 initial points plus the 300 points found by the optimization) to compute the predicted value $\mu(\boldsymbol{\theta})$ and variance $\sigma(\boldsymbol{\theta})^2$. Now we compute the prior density of each point using Eq. (20) and compare $p(\boldsymbol{\theta})$ to a random

variable sampled from a uniform distribution $r \sim \mathcal{U}(0, p_{\max})$. If $p(\theta) > r$, the sample is accepted, otherwise it is rejected. We define the maximum probability $p_{\max}$ to be the prior probability in Eq. (20) evaluated at $\mu(\theta) = y_{\min}$ and $\sigma(\theta)^2 = \min_{\theta \in S}(\sigma^2(\theta))$, that is the minimum variance across the N_s samples of θ. We note that there are potentially higher values of $p(\theta)$. However, this approach led to a higher acceptance rate for samples of the prior distribution, which will be later confirmed to enter the posterior distribution. Now our task is to select N_f final samples that can be used as models of the patient's Purkinje network. According to the ABC methodology, we need to define a distance function between the data and the model to accept or reject samples from the prior distribution. First, we consider that there is some inherent variability in the ECG of each patient. To take into account these variations, we define a distribution $q(e;\theta)$ of errors e that is calculated as the error of each of the N_b beats that we have available for a patient and the ECG predicted by the model with parameters θ. Then, we define our distance function as the total variation distance (Devroye et al., 2018) between the distribution obtained with $\theta_{\min}$ and any other point θ:

$$D(\theta, \theta_{\min}) = \frac{1}{2} \int_0^{\infty} \left| q(e;\theta) - q(e;\theta_{\min}) \right| \mathrm{d}e. \tag{21}$$

We note that we only have samples of q, thus we employ the kernel density estimation function implemented in `scikit-learn` (Pedregosa et al., 2011) with a Gaussian kernel to estimate the integral in Eq. (21). We use cross-validation to obtain the optimal bandwidth of the kernel. We also note than using a traditional squared distance between the prediction and all the measured signals would disregard all the information regarding the QRS variability, as this approach is equivalent to minimizing a distance to the mean QRS signal.

With ABC algorithm completely specified, we proceed to estimate the posterior distribution. First, we sort the samples previously accepted by descending prior probability $p(\theta)$. Then, for each set of parameters θ we compute the forward ECG model and evaluate its error distribution $q(e;\theta)$. Now, we compute the distance between the predicted ECG and the best ECG. We accept the sample θ if $D(\theta, \theta_{\min}) < 0.9$. We repeat this process until we accept $N_f = 30$ posterior samples, a number selected to obtain an estimate of the posterior distribution in a reasonable time. If we reject 50 consecutive samples, we retrain the Gaussian process surrogate including all the new points calculated and we repeat the prior and posterior sampling.

2.6. Patient's data

The proposed model is retrospectively tested with the data from four heart failure patients, which includes a 12-lead ECG and a clinically indicated cardiac magnetic resonance (CMR) scan with late gadolinium-enhancement (LGE) for scar detection. Clinical data and model construction has been previously described (Maffessanti et al., 2020; Pezzuto et al., 2021). The institutional review board approved the study protocol, and all patients gave written and oral informed consent for the investigation. The study was performed in compliance with the Declaration of Helsinki.

Patient anatomies (heart, torso, lungs, major blood masses) were semi-automatically reconstructed from the CMR images. Surfaces of relevant anatomical structures were constructed from their contours using Blender (The Blender Foundation). The outline of the ventricles was detected from short-axis cine images. Scarred tissue was inferred from LGE-MRI sequence by manual contour and alignment. The cardiac anatomy was eventually discretized to create 1-mm resolution 3D volumetric computational grid. Ventricular fiber orientation was assigned using a rule-based approach (Potse et al., 2014).

The 5-minute ECG was recorded using a clinically available ECG machine (CS200 excellence, Schiller AG) having a sampling rate of 1000/s and an amplitude resolution of 1.0 μV. We pre-processed the ECGs as follows. We detected all beats in the recording, using the Pan–Tompkins algorithm (Pan and Tompkins, 1985); we aligned the beats using the R-wave peak; we applied a linear detrend to each beat to correct the baseline; we manually excluded extra-systoles and poor signals; we estimated the mean and standard deviation for each lead. The target QRS complex was then isolated by manually detecting its approximate onset and duration. This approach allowed the cross-correlation to effectively match the QRS complex in the predicted signals, focusing on the area of interest.

For all patients, the values for the intra-/extra-cellular conductivities are: $\sigma_l^i = \sigma_l^e = 3.0\,\mathrm{mS\,cm^{-1}}$, $\sigma_t^i = 0.3\,\mathrm{mS\,cm^{-1}}$, $\sigma_t^e = 1.2\,\mathrm{mS\,cm^{-1}}$, and α is a patient specific value 0.05 to 0.1. We set the conductivities of scarred tissue to 0.

3. Results

We test our method with two experiments: a synthetic example and 4 datasets of real patients. We finalize by simulating conduction system pacing from resynchronization therapy in the 4 patients.

3.1. Synthetic case: left bundle branch block

First we test the model in a synthetic example, where the reference ECG is obtained with the forward ECG model applied in a known Purkinje network. To create the reference network we choose the parameters given by the minimum $\theta_{\min}^{\text{pat1}}$ found by the optimization with the data of patient 1, using the method described in Section 2.4. We select this approach in order to avoid the creation of a network with random parameters, which could lead to a non-realistic reference ECG. We randomly perturb the parameters within a range $\pm 5\%$. Then, the parameters of the reference network are initial lengths of 34.82 mm (LV) and 80.84 mm (RV), fascicles lengths of 9.36 and 18.78 mm (LV) and 44.62 and 11.33 mm (RV), fascicles angles of 1.41 and 2.43 rad (LV) and 2.46 and 2.44 rad (RV), a root time of 73.93 ms in the left ventricle and a conduction velocity of 2 m/s, where LV and RV indicate the parameters of the left and right ventricles, respectively. With these network parameters and the forward ECG model we construct the reference ECG, to which we add Gaussian noise, with a standard deviation of 0.05 mV. Then we perform the optimization and the steps previously described.

After running the entire pipeline, including the posterior distribution estimation, we obtain the results of the synthetic case in terms of activation time maps and predicted ECGs, shown in Fig. 3. The distribution of the parameters of the networks selected is shown in the pair plot of Fig. 4. The activation time maps of the reference network and the best point found by the optimization have very close pattern and values. Regarding the 30 inferred networks, the predicted ECGs are similar to the reference ECG, with similar curves in all leads. Additionally, the pair plot shows that the parameters of the right ventricle (initial length, fascicles lengths, fascicles angles) along with the root time and conduction velocity are concentrated around the reference values, while the other parameters are evenly distributed in their respective ranges. The different distributions of the parameters show that some of them can be easily identified, while other cannot. The lack of identifiability of the parameters of the left ventricle has a physiological explanation: the simulated patient has a left bundle branch block (root time of 75 ms in the left ventricle) and the activation of the left ventricle is coming directly from the right ventricle. This effect can be clearly observed in Fig. 3a, where the earliest activation occurs on the right ventricle and propagates towards the left ventricle. Thus, there is little effect of the left Purkinje tree on the ECG, and multiple combinations of parameters will explain the data. The variety of inferred Purkinje trees can be seen in Fig. 5, where we present the reference network along with 15 random networks and 15 of the selected samples, which show the different activation patterns that the networks may produce, and how the model selects different networks that produce similar ECGs.

In the Appendix B we show a synthetic example, where the reference Purkinje network is constructed with the same parameters $\theta_{\min}^{\text{pat1}}$, but we set the root time to 0 ms, so both ventricles are activated at the same time.

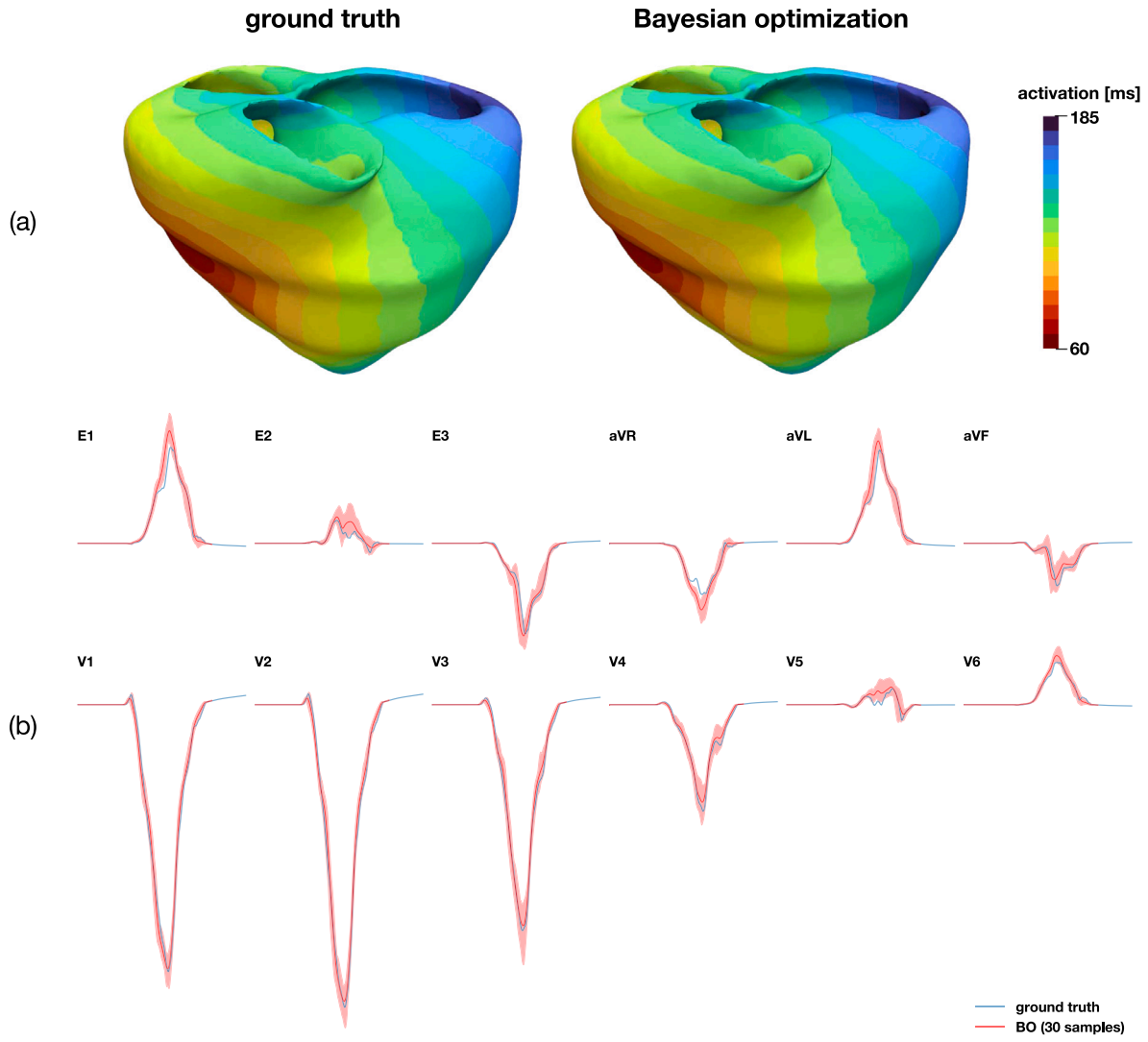

Fig. 3. Synthetic results. (a) Activation time maps for the ground truth and the best network found by the optimization. (b) Reference ECG (in blue) and ECGs of the 30 networks found by the method (in red), with the mean in a solid red line and the area between the minimum and maximum values of each time step shaded.

3.2. Patient data

Now we use the proposed model to find Purkinje networks that describe the ECG of each patient. The optimization for patients 1, 2, 3, and 4 found minima with MSE 0.433 mV^2, 0.348 mV^2, 0.564 mV^2, and 0.937 mV^2, respectively. Then, the ABC algorithm found the 30 posterior samples for each patient, with the predicted ECGs shown in Fig. 6. From this figure it can be observed that the model correctly captures the behavior of each patient's ECG. Moreover, the variability in the predicted ECGs is in the same scale as the inherent variability of the reference ECGs, depicted by the blue band. However, the results show that the model struggles to capture some of the low-amplitude leads, such as V5 and V6.

The pair plot of Fig. 7 shows the distribution of the parameters of the selected networks of each patient. Note that some parameters are evenly distributed in their respective ranges, as the fascicles lengths in the left ventricle, which indicates that their values do not have an important effect in the ECG, since regardless of their values an ECG similar to the reference can be obtained. In contrast, other variables are concentrated in certain regions. For example, the root time tends to have negative values, especially for patients 3 and 4, indicating a later activation of the left ventricle that may be caused by left bundle branch block. For some variables the distribution depends on the patient, for example, for the conduction velocity the patients 1 and 4 (in blue and purple, respectively) are concentrated in the lower values, while the patients 2 and 3 (in orange and green) present values throughout the range, reflecting the characteristics of each patient. Considering this, the parameters that can be identified from the data highly depend on the patient. For instance, patient 3 shows a concentrated distribution for the first fascicle length of the right ventricle, while patients 2 and 4 show a similar behavior for initial length of the right ventricle and the right fascicle angles.

3.3. Conduction system pacing simulation

The result of the proposed method is a set of Purkinje networks that can be used to predict a patient ECG under certain conditions or treatments. As a proof of concept here we simulate cardiac resynchronization therapy (Verzaal et al., 2022), which is treatment used in heart failure patients, such as the ones in this study. To highlight the potential of the method and specially of the uncertainty estimates, we attempt to recreate His–Purkinje conduction system pacing, where the pacemaker lead directly activates the Purkinje network to synchronize both ventricles (Vijayaraman et al., 2023). We remark that we do

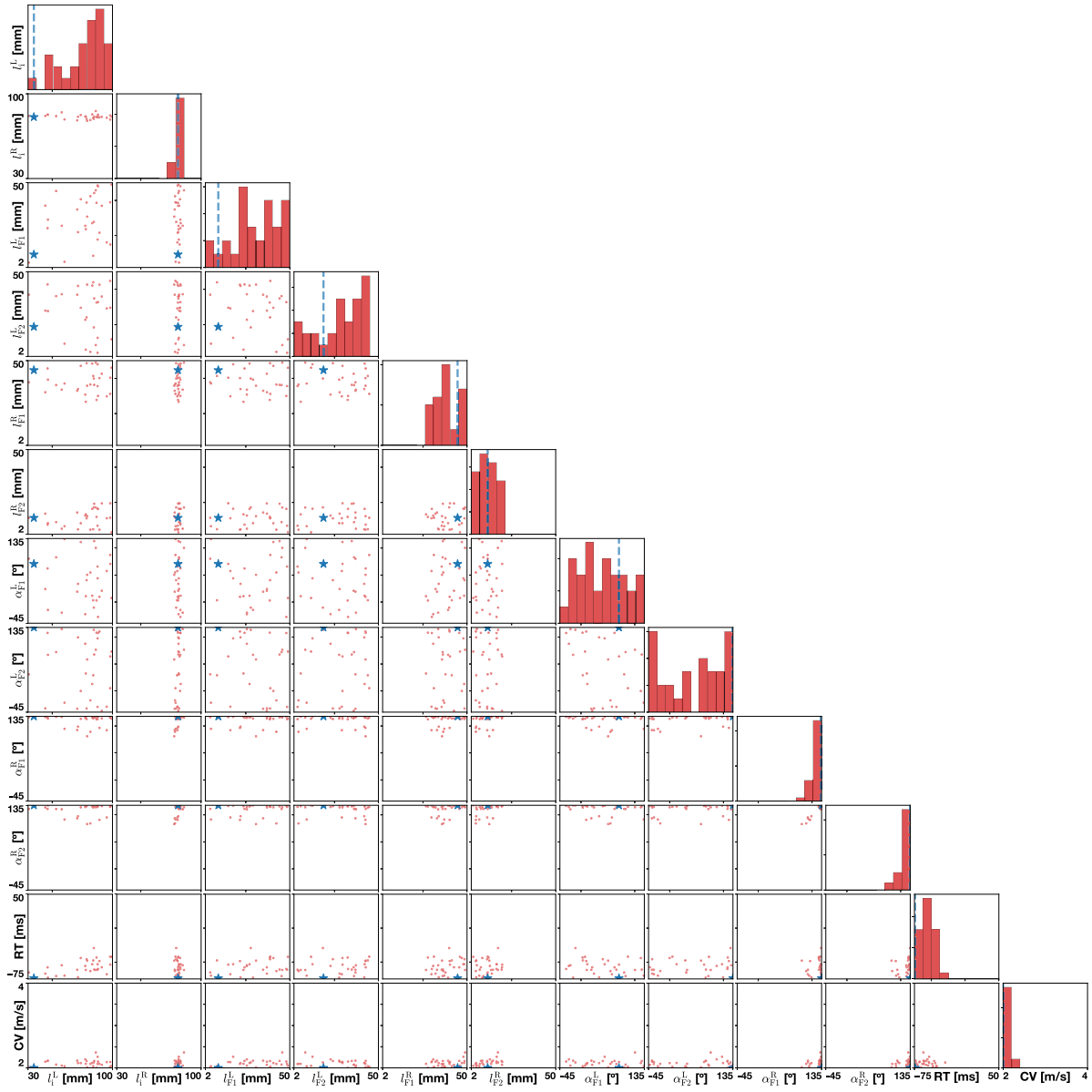

Fig. 4. Synthetic results: left bundle branch block. Each of the samples that the model produces corresponds to a set of ten geometric parameters (to determine the shape of the Purkinje network) and two electrophysiology parameters (root time and conduction velocity). The pair plot in this figure shows the distribution of the parameters of the reference network (in blue) and the 30 inferred networks (in red). Each parameter is represented once in a row of the y-axes, and once in a column of the x-axes; then the diagonal shows the distribution of each variable, and the off-diagonal plots show the correlation between two different variables.

not attempt to establish the effectiveness of this therapy, we are only simulating its effect on cardiac activation and the ECG.

In order to simulate conduction system pacing, we take the selected networks of each patient and set the root time to 0 ms, synchronizing the activation of the left and right trees. Then, we have 30 simulations for each patient. For clarity, Fig. 8 shows the activation maps of only three samples per patient. To appreciate the variability, we found the largest activation time for each sample, sorted them by this value, and selected the samples with the minimum, median and maximum value for display. We see that for patient 2, the activation maps show little variation, always displaying a right to left activation. Patient 4 shows a larger variation, but the earliest activation is located in the right ventricle in all cases. On the other hand, patients 1 and 3 show a larger variation in the activation maps. This is reflected in Fig. 9, which shows the predicted ECGs for this simulation. Patients 1 and 3 show a much larger variability in the ECGs than patients 2 and 4. These results highlight the importance of taking a probabilistic approach, such that uncertainties in the predictions can be quantified.

4. Discussion

We have presented a novel method to identify the Purkinje network from the ECG. This tool combines advanced machine learning techniques, with advanced cardiac electrophysiology modeling and statistical tools. We have developed a novel algorithm, based on the idea of harmonic maps, to generate the Purkinje network that is more efficient and numerically stable than previous attempts. We also propose an approach to couple the Purkinje network with the myocardium efficiently. Finally, we design a custom algorithm combining Bayesian optimization with approximate Bayesian computation to infer a distribution of Purkinje networks that can explain the data. This point is particularly important in a clinical setting (Quaglino et al., 2018), where uncertainties are large and making a decision based on a single plausible, but incorrect model can have dangerous consequences. We have tested our methodology in synthetic examples and patient's data.

The synthetic example showcases that our pipeline is able to recover a ground truth parameters distribution, serving as a numerical

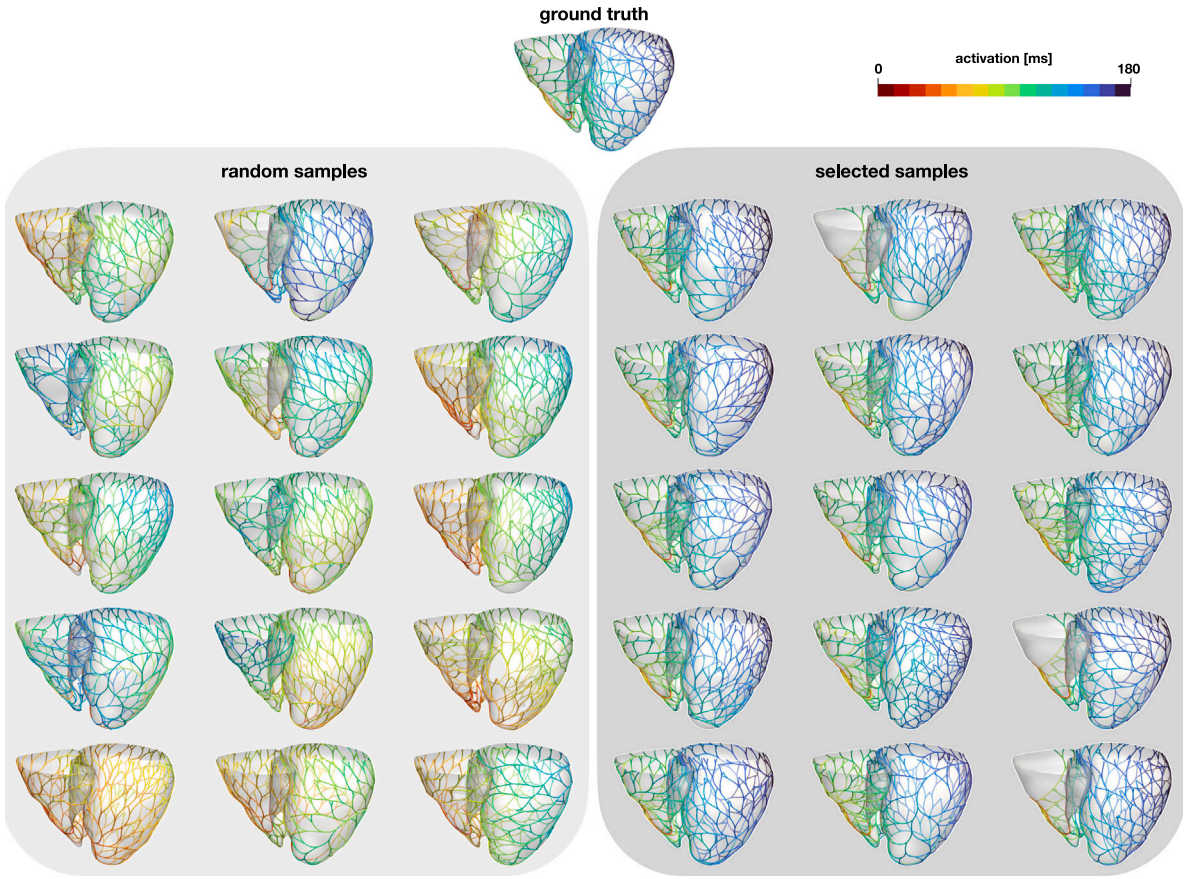

Fig. 5. On top, the reference Purkinje network for the synthetic example with left bundle branch block. (left) 15 random networks, created within the respective range of each parameter. (right) 15 of the inferred samples by the model. In colors the activation times of each network.

validation. More importantly, it highlights that recovering the Purkinje network solely from the ECG is an ill-posed problem with manifold solutions, as different combinations of parameters resulted in very similar ECGs. Moreover, portions of the Purkinje tree can become undetectable from the ECG, especially in the case of bundle branch block. Our method can detect this issue, which results in a large spread in the posterior distribution of the parameters.

In our tests with patient's data, we show that our methodology can recover the specific ECGs of each case. The posterior distribution of the parameters shows that there is a large variability on the parameters of the Purkinje network for the different patients. The ECGs of the patients also show some variability, which may explain the difference in parameters. The results of the posterior distribution also show that the parameters that can be identified depend on the patient, thus it would not be easy to eliminate a priori some parameters from the analysis. Nonetheless, a large uncertainty in some of the parameters does not necessarily imply a large uncertainty in the activation map. Therefore, the ECG-based posterior distribution could be a valuable clinical tool, for instance in the detection of the latest activated area or potential targets for lead placement (Ellenbogen et al., 2023).

Our approach contains several advantages over existing methods for reconstructing the Purkinje network from the ECG (Kahlmann et al., 2017; Gillette et al., 2021a; Camps et al., 2024). Firstly, our reconstruction of the network is probabilistic, rather than a pointwise estimate. Given the ill-posedness of the inverse problem, a posteriori uncertainty quantification must be provided in order to render the results reliable for the clinical decision making. Secondly, our method does not necessitate the two-step procedure for estimating the early activation sites first, and then growing the network through the sources. In general, the ECG produced after the second step does not match 1:1 the fitted ECG, because the Purkinje network introduces more sources and some junctions could be activated retrogradely. Moreover, a high number of junctions like in our case can better capture more complex activation patterns and fit the ECG more faithfully.

The cardiac resynchronization therapy study highlights a potential clinical application of our method. Here, we can use the inferred network to predict the activation patterns and ECGs after the application of a conduction system pacing. Coupled with a mechanical model, this tool could be used to quantify changes in ejection fraction for a given treatment (Lee et al., 2018). But more importantly, this application shows the importance of estimating a distribution of Purkinje networks rather than a point estimate. In this way, we can estimate how informative the data are, and thus our level of trust in our predictions. We saw in two out of four patients that the uncertainties in the predicted ECGs were large, predominantly caused by the large uncertainties in the parameters of the left Purkinje tree, which is not contributing to the surface ECG. Thus, when the left Purkinje tree is activated with the pacing, the resulting activation patterns are highly variable.

Our work presents some limitations. We use a simplified and idealized representation of the Purkinje network. However, from a modeling perspective, it is complex enough to represent the ECG of the patients that we studied. We even fixed some of the parameters such as the branch length, angle, the repulsive parameter and the myocardium conduction velocity because we observed that we could still fit the ECG with these simplifications. We found this step to be critical to reduce the dimensionality of the problem and perform a successful optimization. In this sense, we do not claim that we can reconstruct the actual geometry of the Purkinje network, but a functional model of it. Another limitation is that creating the heart and torso model can be time consuming, thus it limits the clinical usability of our approach. However, deep learning techniques have greatly accelerated this process, making it possible to go directly from an image to the

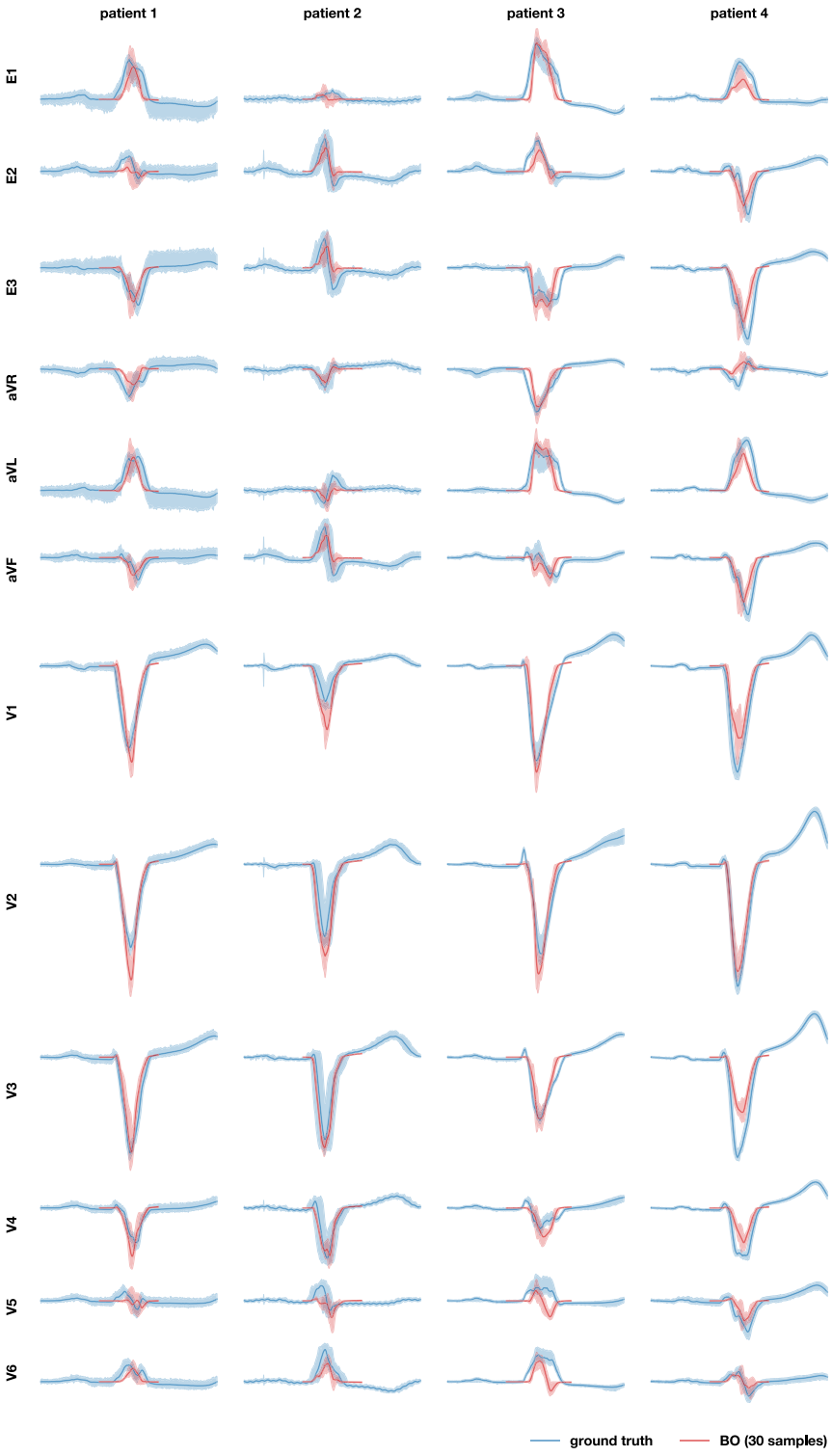

Fig. 6. ECGs for the four patients analyzed. In a solid blue line the mean of the beats of the signal, which is the reference used in the optimization to compare the predicted ECGs. We also show in the shaded blue area the difference between the minimum and maximum values of the signal of every beat. In red, the predicted ECGs of the 30 selected samples, with the mean in a solid red line and the area between the minimum and maximum value of each time step shaded. The shaded blue and red areas allow to compare the intrinsic variability in the beats of the ECG signal, with the different ECGs predicted by the selected samples.

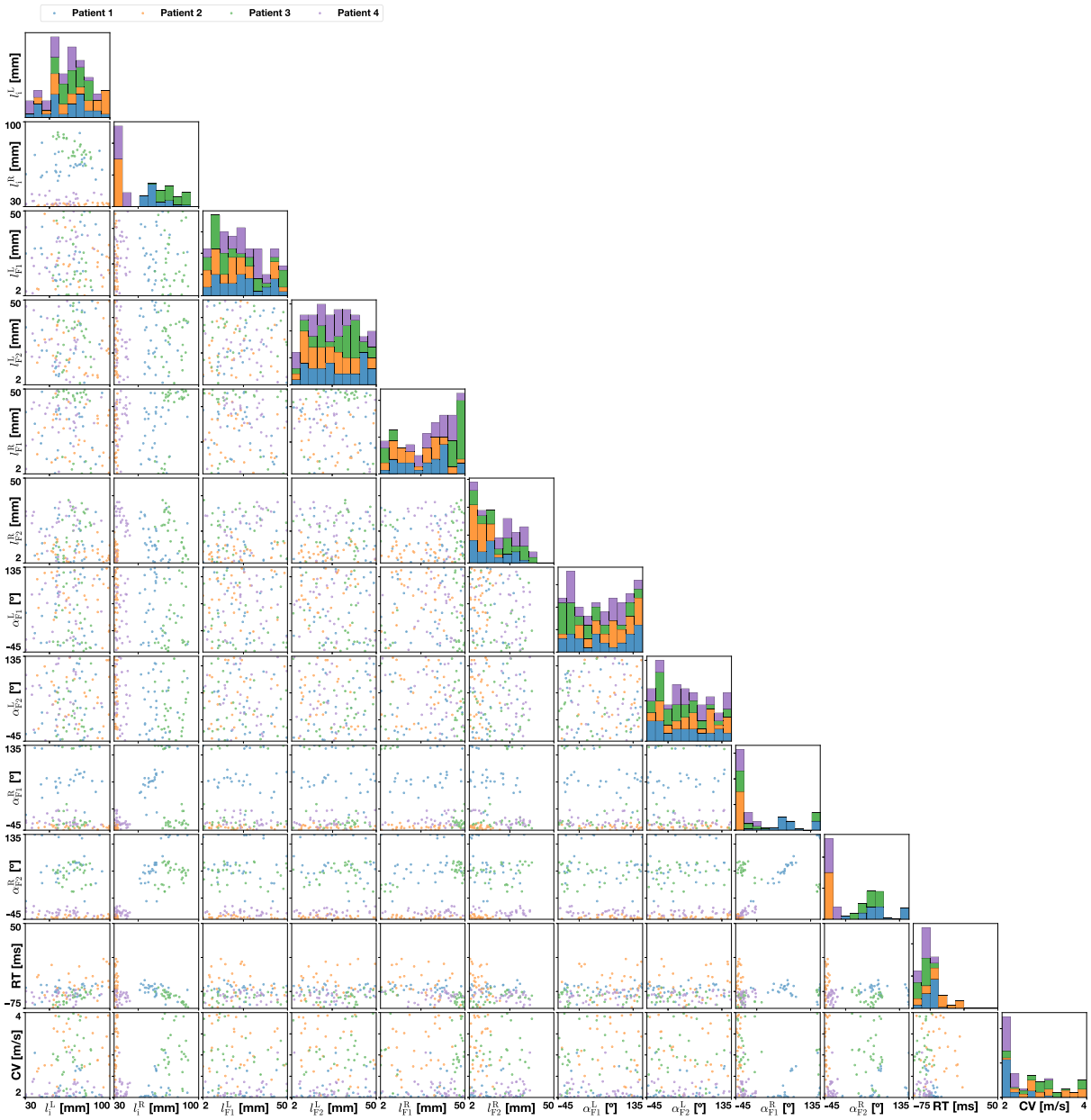

Fig. 7. Distribution of parameters of the selected samples for each patient. Patients 1, 2, 3, and 4 are represented by the colors blue, orange, green and purple, respectively. For each of them, the model selects 30 networks that produce ECGs similar to the patient's. Every network is characterized by 12 parameters, which are represented in the rows and columns of the pairplot, showing their relationship and distribution.

model (Kong and Shadden, 2022). Regarding the computational cost to perform the inference of the Purkinje network, it took around 15 h per patient, for the entire process. Since this is a process that can be done offline after the ECG and the images are acquired, it does not limit the clinical applicability. Nonetheless, the current implementation is not optimized and the computational time could be reduced by several hours. For instance, the Purkinje network generator is not optimized and written in plain Python. This process currently takes much longer than solving the Eikonal equation on the entire heart, which is based on a code that is highly optimized for GPU (Pezzuto et al., 2017; Grandits, 2021). Furthermore, we could run multiple models in parallel for the initial training set of the Gaussian process and for the approximate Bayesian computation. Another limitation is that we have used an Eikonal model for ventricular and Purkinje activation. However, studies have shown that error introduced by the eikonal approximation is fairly small (Neic et al., 2017) and can be further reduced with an eikonal-diffusion model (Gander et al., 2023). Importantly, we do not account for a realistic Purkinje-muscle junction (Vigmond and Stuyvers, 2016). The activation delay at the junctions could be introduced explicitly in the eikonal model (Vergara et al., 2016). Also, we have only calibrated the QRS complex, excluding the T-wave. Although this is a simplification, we believe is the only way to keep the problem tractable, as the morphology of the T-wave is due to spatial heterogeneities of the action potential duration and is difficult to capture with an eikonal model. Nonetheless, once we have estimated the Purkinje network, we could regionally modify the model for the action potential to fit the T-wave as well (Verzaal et al., 2022). We plan to do this in the future. Finally, we need to validate if the learned Purkinje networks can reproduce other activations. We plan to do this in the future, but acquiring such data is challenging as it would require an invasive procedure to pace the ventricles from a different site.

Overall, we believe the presented methodology provides a solid step to learn the Purkinje network from the ECG with quantified uncertainties. We hope it will improve the way that digital twins for cardiac

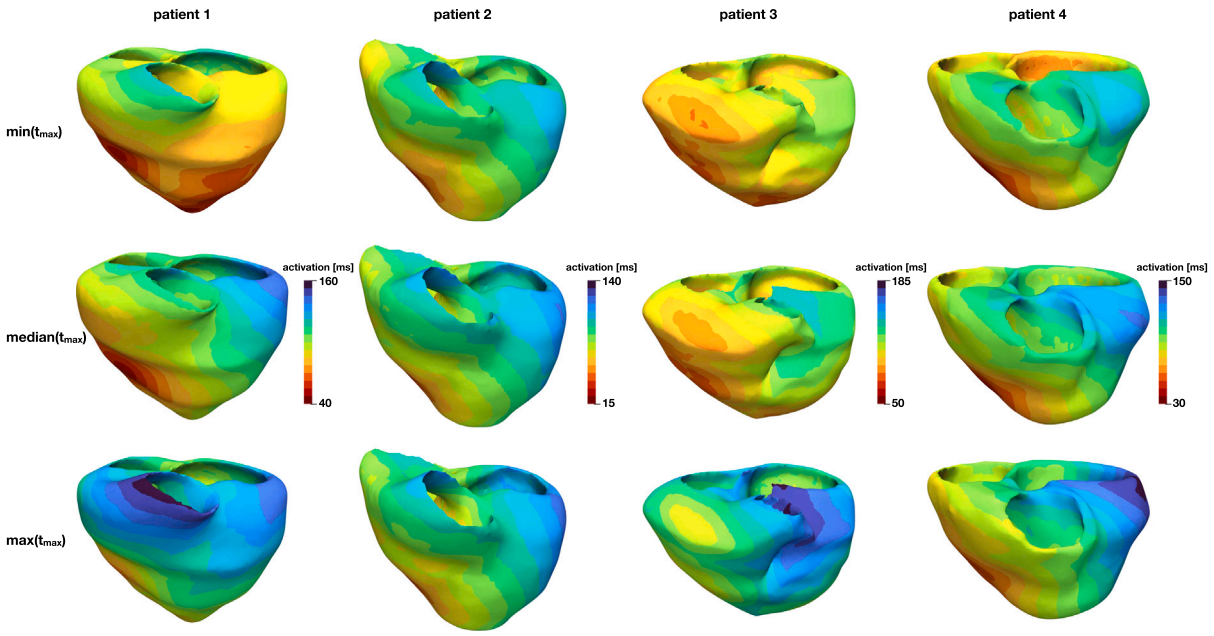

Fig. 8. Activation time maps for the pacemaker simulation. For the pacemaker simulation we take the 30 selected networks of each patient and set the root time to zero. Here we show the activation maps of three samples per patient: for each of the 30 maps we find the largest activation time and sort the samples according to their value, then we show only the samples with the minimum, median and maximum of this value.

electrophysiology are created, leading into more precise diagnosis and effective treatment for patients.

CRediT authorship contribution statement

Felipe Álvarez-Barrientos: Writing – original draft, Software, Methodology. **Mariana Salinas-Camus:** Software. **Simone Pezzuto:** Writing – review & editing, Writing – original draft, Validation, Software, Investigation, Funding acquisition, Data curation, Conceptualization. **Francisco Sahli Costabal:** Writing – review & editing, Writing – original draft, Supervision, Software, Project administration, Funding acquisition, Conceptualization.

Declaration of competing interest

The authors declare that they have no known competing financial interests or personal relationships that could have appeared to influence the work reported in this paper.

Acknowledgments

This work was funded by ANID – Millennium Science Initiative Program – ICN2021_004 and National Center for Artificial Intelligence CENIA FB210017, Basal ANID to FSC. FSC and FAB and also acknowledges the support of the project FONDECYT-Iniciación 11220816 and ERAPERMED-134 from ANID. SP acknowledges the support of the CSCS-Swiss National Supercomputing Centre project no. s1275, the PRIN-PNRR project no. P2022N5ZNP and the Swiss National Science Foundation (SNSF) grant 214817.

Appendix A. Bayesian optimization: Why we choose 250 initial data points and 300 steps for the optimization?

For the Bayesian optimization we had to select two quantities: the number of points where we execute the forward ECG model to obtain the initial dataset, and the number of steps for the optimization. Ideally, both numbers should be as high as possible, which allows a better knowledge of the function and its minimum (or minimums), however, as each of they increase, the computational cost also increases. Then, the task is to balance both aspects. In this work we choose to execute the forward ECG model to sample 250 points with Latin hypercube sampling, and then we perform the optimization for 300 steps. The selection of these quantities is based on the results of the optimization: Fig. A.10 shows that the minimum value is reached at iteration 276 for patient 1, iteration 186 for patient 2, iteration 242 for patient 3, and iteration 101 for patient 4. Therefore, we expect that increasing the initial dataset or the optimization steps will not produce a significant improvement on the minimum found.

Appendix B. Synthetic case: ground truth values in the middle of each range

In this example, we use the proposed model to recover an artificial ECG, computed using the anatomy of the heart of patient 1 and an artificially created Purkinje network, where each of the geometrical and electrophisiology parameters is set to the midpoint of its respective range. Thus, the reference network parameters are initial lengths of 65 mm for both the left and right ventricles (LV and RV), fascicles lengths of 26 mm (LV and RV), fascicles angles of 0.79 rad (LV and RV), a root time of 12.5 ms in the left ventricle, and a conduction velocity of 3 m/s. Then, with the forward ECG model we compute the reference ECG, to which we add Gaussian noise with a standard deviation of 0.05 mV, leading to an average signal to noise ratio of 9.5 dB.

Applying the optimization and the ABC algorithm, we found the minimum and then the selected samples, which broadly resemble the reference ECG. Fig. B.11a shows the reference activation time map along with the map of the minimum found by the optimization. Both maps show an activation from the right to the left ventricle, but with some differences, particularly in the left ventricle. Fig. B.11b compares the reference ECG and the ECGs of the selected samples, which accurately capture the reference behavior, especially in the leads with high amplitude, such as V1, V2, V3, and V4.

Despite the similarity in the simulated ECGs, the pairplot in Fig. B.12 reveals high variability in the selected samples, with different combinations of geometrical and physiology parameters. For example, the values of the fascicles lengths $l^{\mathrm{L}}_{\mathrm{F1}}$, $l^{\mathrm{L}}_{\mathrm{F2}}$, $l^{\mathrm{R}}_{\mathrm{F1}}$, fascicles angles $\alpha^{\mathrm{L}}_{\mathrm{F1}}$, $\alpha^{\mathrm{L}}_{\mathrm{F2}}$ are approximately evenly distributed within their ranges. The fascicle length $l^{\mathrm{R}}_{\mathrm{F2}}$ and the conduction velocity present values in the lower half

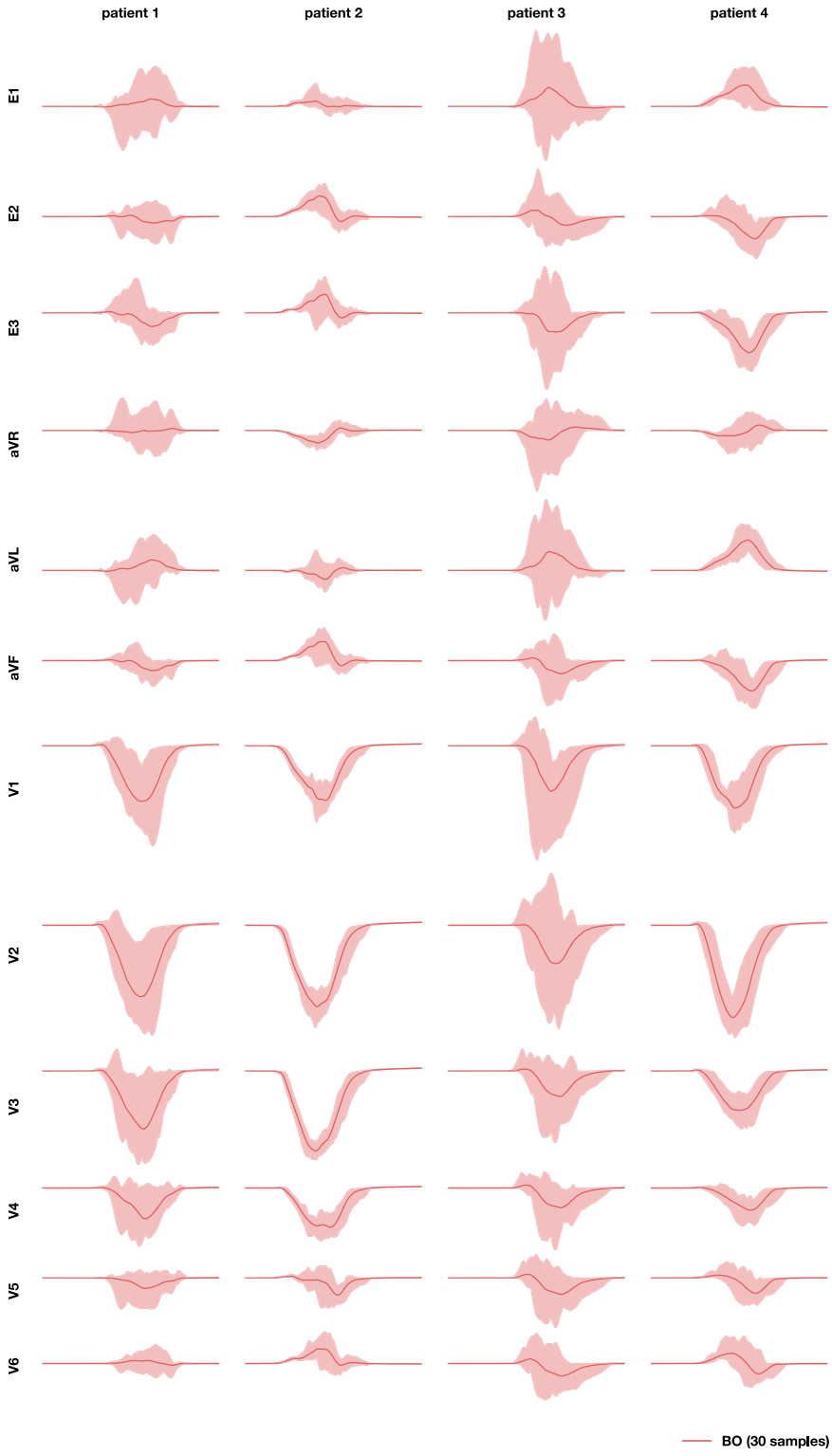

Fig. 9. ECGs of the pacemaker simulation. In red, the predicted ECGs of the 30 selected samples of each patient, with the mean in a solid red line and the area between the minimum and maximum value of each time step shaded.

of their ranges, while the initial length l_i^L, fascicles angles α_{F1}^R, α_{F2}^R, and the root time in the upper half. Only the initial length l_i^R exhibit values around the reference value. However, consistent with the simulated ECGs, the selected samples show similar behavior to the reference. This is illustrated in Fig. B.13, which displays the reference network, 15 random samples and 15 of the selected samples. The random samples exhibit diverse behaviors, while in general the selected samples show a later activation of the left ventricle, consistent with the ground truth.

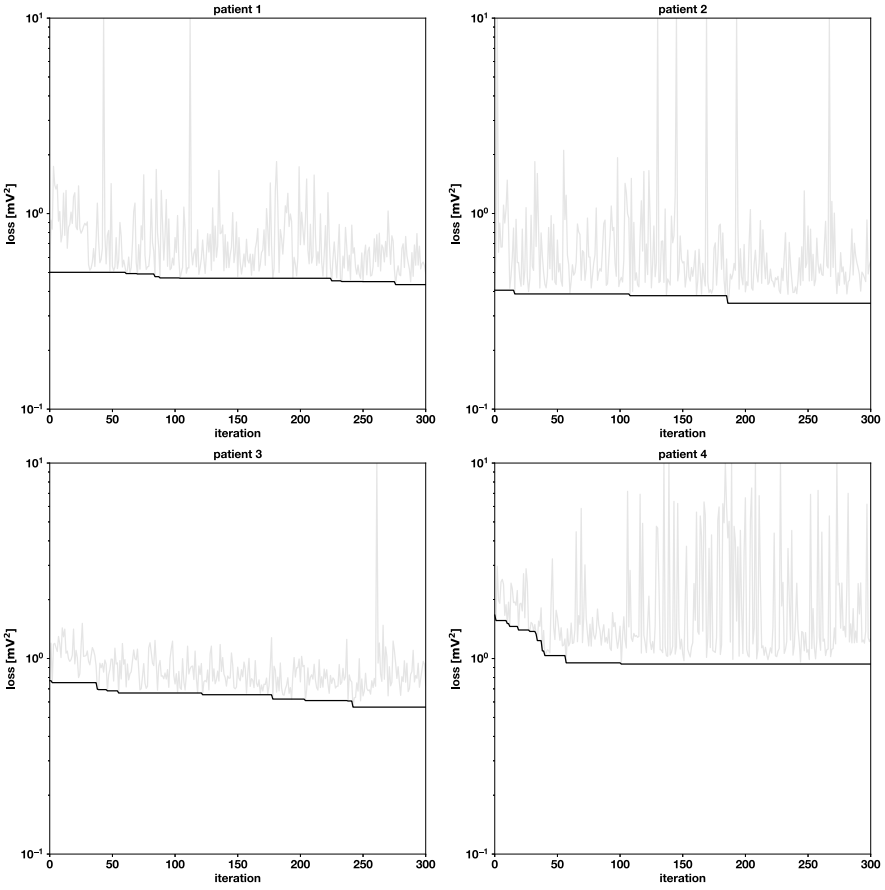

Fig. A.10. Loss function during optimization. The Figure shows the loss function value over the 300 iterations of the Bayesian optimization. The initial value corresponds to the minimum of the initial dataset. The solid line represents the minimum value reached up to that number of iterations and the gray line shows the value of the loss function of the acquired sample at each iteration. The minimum value is reached at iteration 276 for patient 1, iteration 186 for patient 2, iteration 242 for patient 3, and iteration 101 for patient 4.

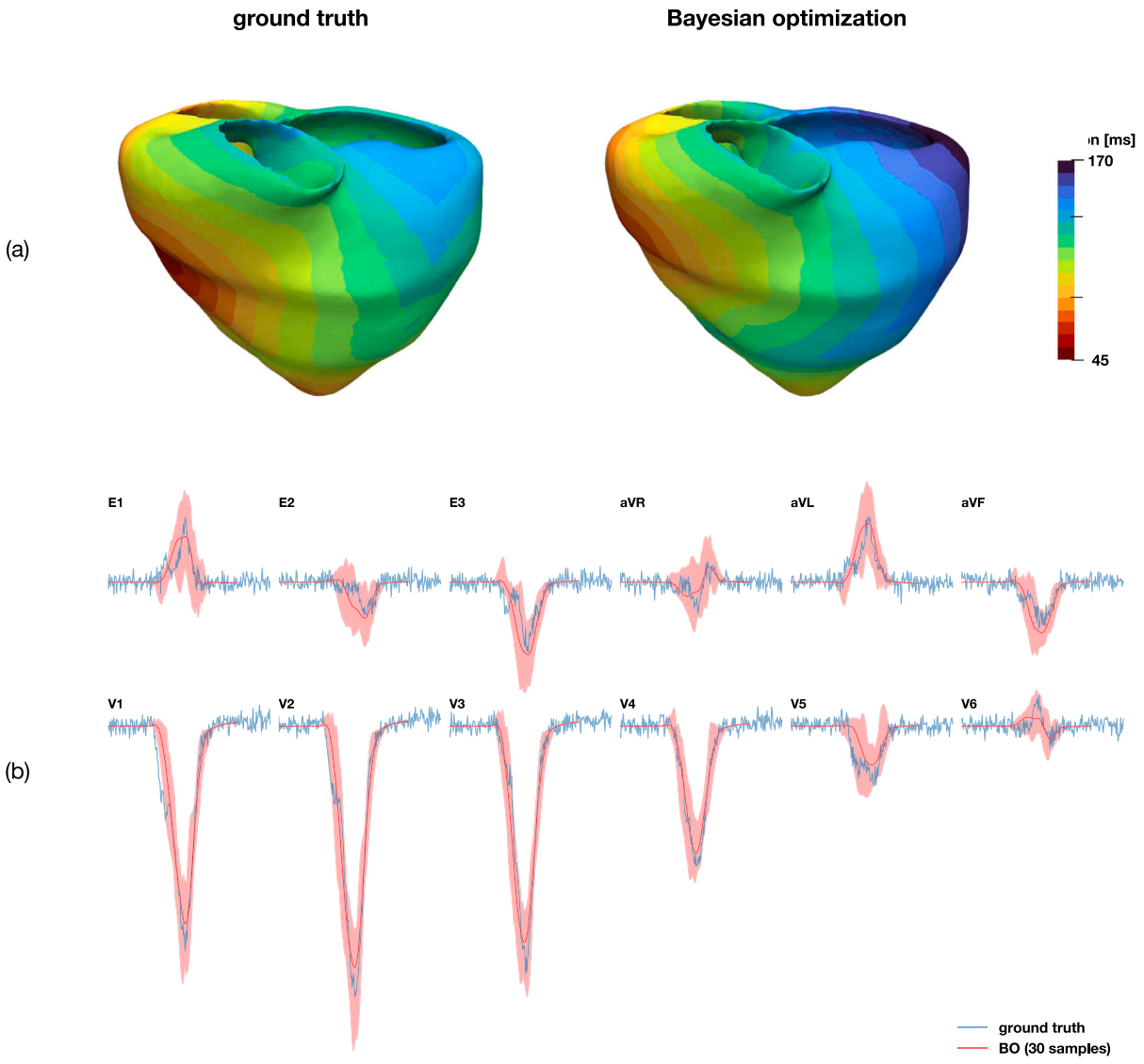

Fig. B.11. Synthetic results: ground truth values in the middle of each range. In this example we take the anatomy of patient 1, and create an artificial reference Purkinje network, setting each of the geometrical and electrophisiology parameters in the middle of each range. Then, with the forward ECG model we compute the reference ECG. The proposed model allows us to find 30 samples that generate similar ECGs. In (a) we show the activation time maps for the ground truth and the best network found by the optimization. Then, in (b) the reference ECG (in blue) and ECGs of the 30 networks found by the method (in red), with the mean in a solid red line and the area between the minimum and maximum values of each time step shaded.

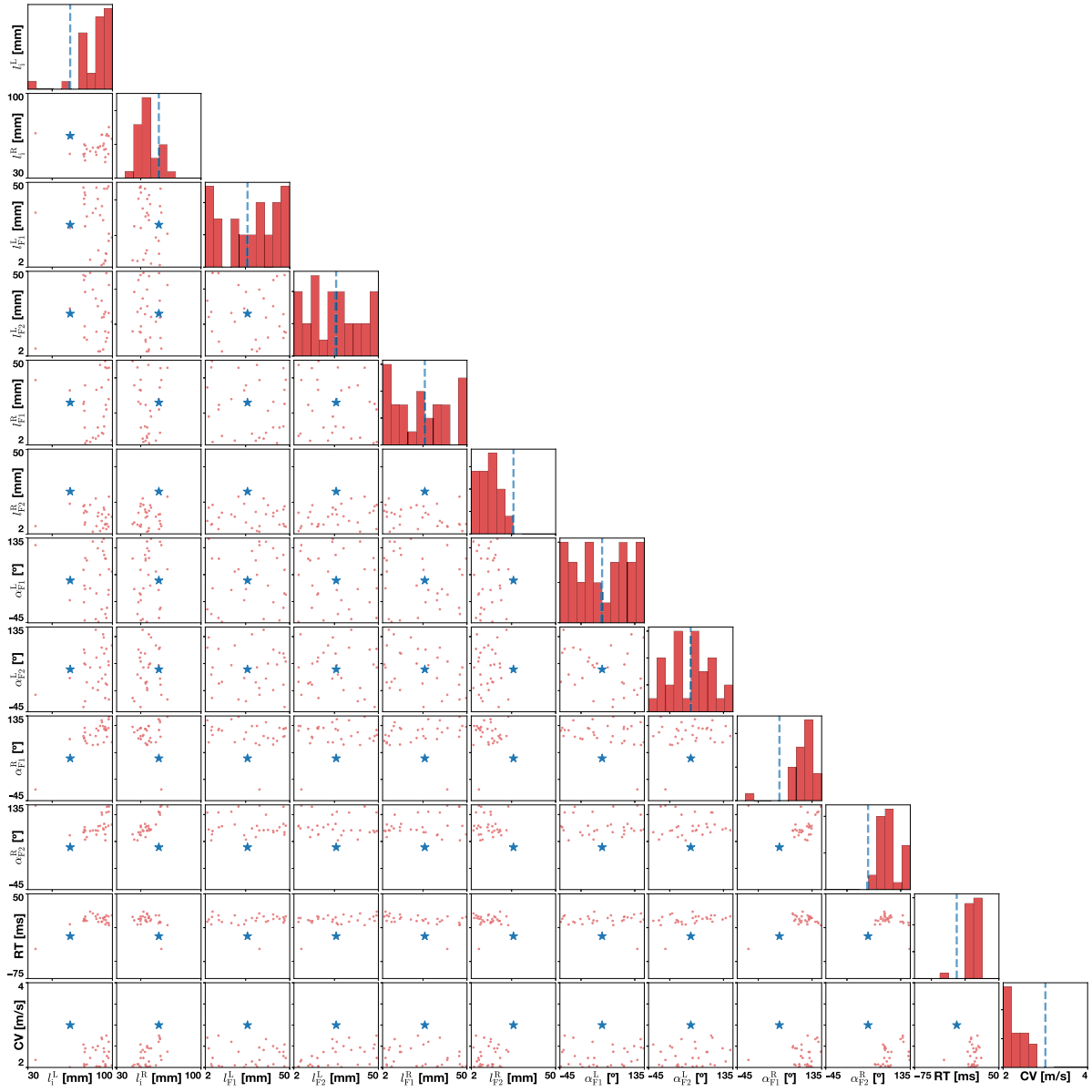

Fig. B.12. Synthetic results: ground truth values in the middle of each range. Each of the samples that the model produces corresponds to a set of ten geometric parameters (to determine the shape of the Purkinje network) and two electrophysiology parameters (root time and conduction velocity). The pair plot in this Figure shows the distribution of the parameters of the reference network (in blue) and the 30 inferred networks (in red). Each parameter is represented once in a row of the y-axes, and once in a column of the x-axes; then the diagonal shows the distribution of each variable, and the off-diagonal plots the relationship between two different variables.

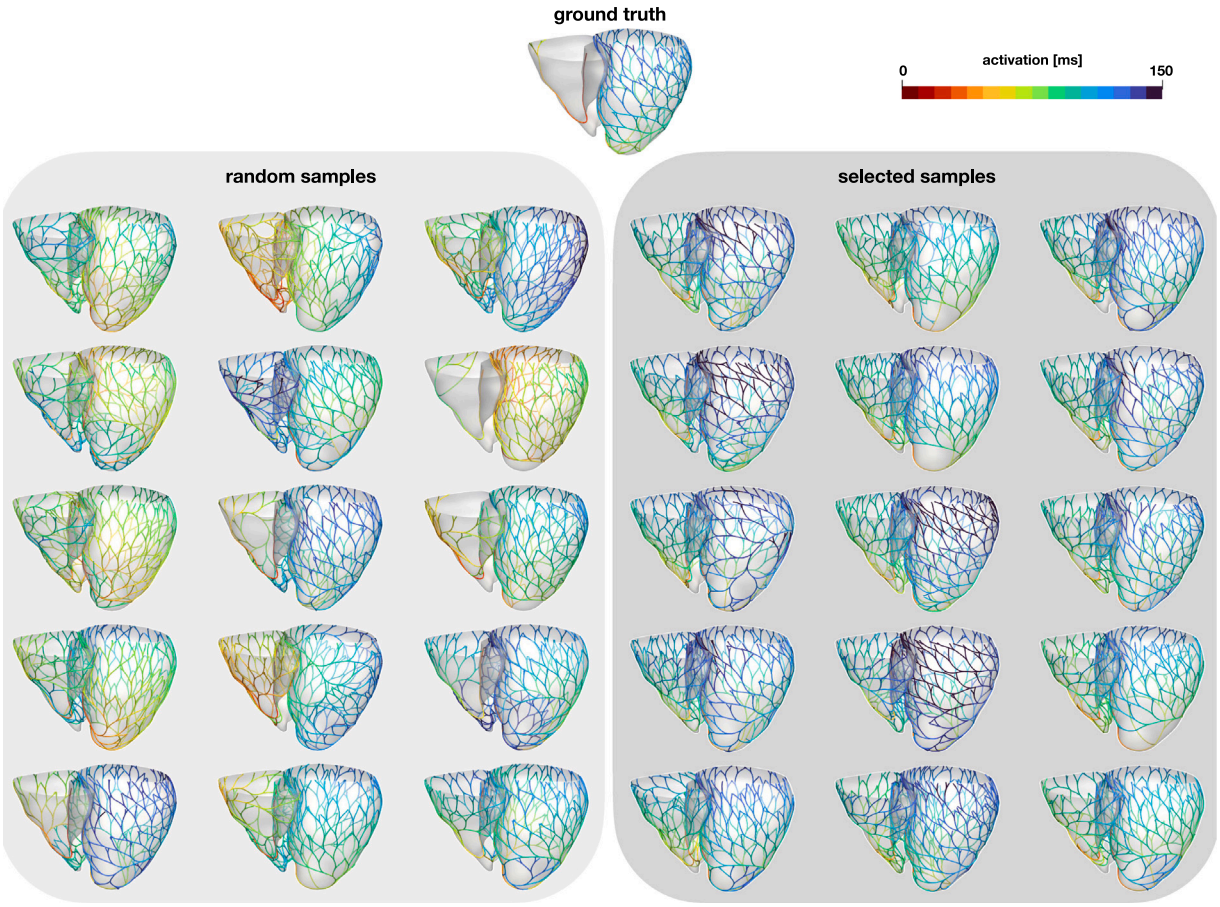

Fig. B.13. On top, the reference Purkinje network for the synthetic example with ground truth values in the middle of each range. (left) 15 random networks, created within the respective range of each parameter. (right) 15 of the inferred samples by the model.

Data availability

The patient data is confidential, but an open source implementation with a synthetic example is provided at: http://github.com/fsahli/purkinje-learning.

References

Barber, F., Langfield, P., Lozano, M., García-Fernández, I., Duchateau, J., Hocini, M., Haïssaguerre, M., Vigmond, E., Sebastian, R., 2021. Estimation of personalized minimal purkinje systems from human electro-anatomical maps. IEEE Trans. Med. Imaging 40 (8), 2182–2194.

Berg, L.A., Rocha, B.M., Oliveira, R.S., Sebastian, R., Rodriguez, B., de Queiroz, R.A.B., Cherry, E.M., Dos Santos, R.W., 2023. Enhanced optimization-based method for the generation of patient-specific models of Purkinje networks. Sci. Rep. 13 (1), 11788.

Blanchard, A., Sapsis, T., 2021. Bayesian optimization with output-weighted optimal sampling. J. Comput. Phys. 425, 109901.

Camps, J., Berg, L.A., Wang, Z.J., Sebastian, R., Riebel, L.L., Doste, R., Zhou, X., Sachetto, R., Coleman, J., Lawson, B., et al., 2024. Digital twinning of the human ventricular activation sequence to clinical 12-lead ECGs and magnetic resonance imaging using realistic purkinje networks for in silico clinical trials. Med. Image Anal. 103108.

Camps, J., Lawson, B., Drovandi, C., Minchole, A., Wang, Z.J., Grau, V., Burrage, K., Rodriguez, B., 2021. Inference of ventricular activation properties from non-invasive electrocardiography. Med. Image Anal. 73, 102143.

Cárdenes, R., Sebastian, R., Soto-Iglesias, D., Berruezo, A., Camara, O., 2015. Estimation of purkinje trees from electro-anatomical mapping of the left ventricle using minimal cost geodesics. Med. Image Anal. 24 (1), 52–62.

Çetingül, H.E., Plank, G., Trayanova, N.a., Vidal, R., 2011. Estimation of local orientations in fibrous structures with applications to the purkinje system. IEEE Trans. Biomed. Eng. 58 (6), 1762–1772. http://dx.doi.org/10.1109/TBME.2011.2116119.

Despotovic, V., Skovranek, T., Schommer, C., 2020. Speech based estimation of parkinson's disease using Gaussian processes and automatic relevance determination. Neurocomputing 401, 173–181.

Devroye, L., Mehrabian, A., Reddad, T., 2018. The total variation distance between high-dimensional Gaussians with the same mean. arXiv preprint arXiv:1810.08693.

Dubin, D., 1996. Rapid Interpretation of EKG's. Cover Publishing Company, 1996, USA.

Ellenbogen, K.A., Auricchio, A., Burri, H., Gold, M.R., Leclercq, C., Leyva, F., Linde, C., Jastrzebski, M., Prinzen, F., Vernooy, K., 2023. The evolving state of cardiac resynchronization therapy and conduction system pacing: 25 years of research at EP europace journal. Europace 25 (8), euad168.

Fu, Z., Kirby, R., Whitaker, R., 2013. A fast iterative method for solving the eikonal equation on tetrahedral domains. SIAM J. Sci. Comput. 35 (5), C473–C494. http://dx.doi.org/10.1137/120881956, URL https://epubs.siam.org/doi/abs/10.1137/120881956.

Gander, L., Krause, R., Weiser, M., Sahli Costabal, F., Pezzuto, S., 2023. On the accuracy of eikonal approximations in cardiac electrophysiology in the presence of fibrosis. In: Bernard, O., Clarysse, P., Duchateau, N., Ohayon, J., Viallon, M. (Eds.), Functional Imaging and Modeling of the Heart. In: Lecture Notes in Computer Science, vol. 13958, Springer, Cham, pp. 137–146. http://dx.doi.org/10.1007/978-3-031-35302-4_14.

Garnett, R., 2023. Bayesian Optimization. Cambridge University Press.

Giffard-Roisin, S., Delingette, H., Jackson, T., Fovargue, L., Lee, J., Rinaldi, A., Ayache, N., Razavi, R., Sermesant, M., 2017. Sparse bayesian non-linear regression for multiple onsets estimation in non-invasive cardiac electrophysiology. In: Functional Imaging and Modelling of the Heart: 9th International Conference, FIMH 2017, Toronto, on, Canada, June 11-13, 2017, Proceedings 9. Springer, pp. 230–238.

Gillette, K., Gsell, M.A., Bouyssier, J., Prassl, A.J., Neic, A., Vigmond, E.J., Plank, G., 2021a. Automated framework for the inclusion of a his–purkinje system in cardiac digital twins of ventricular electrophysiology. Ann. Biomed. Eng. 49 (12), 3143–3153.

Gillette, K., Gsell, M.A.F., Prassl, A.J., Karabelas, E., Reiter, U., Reiter, G., Grandits, T., Payer, C., Štern, D., Urschler, M., Bayer, J.D., Augustin, C.M., Neic, A., Pock, T., Vigmond, E.J., Plank, G., 2021b. A Framework for the generation of digital twins of cardiac electrophysiology from clinical 12-leads ECGs. Med. Image Anal. 71, 102080. http://dx.doi.org/10.1016/j.media.2021.102080, URL https://www.sciencedirect.com/science/article/pii/S1361841521001262.

Goodyer, W.R., Beyersdorf, B.M., Duan, L., van den Berg, N.S., Mantri, S., Galdos, F.X., Puluca, N., Buikema, J.W., Lee, S., Salmi, D., et al., 2022. In vivo visualization and molecular targeting of the cardiac conduction system. J. Clin. Investig. 132 (20).

Grandits, T., 2021. A fast iterative method python package. J. Open Source Softw. 6 (66), 3641.

Grandits, T., Pezzuto, S., Plank, G., 2022. Smoothness and continuity of cost functionals for ECG mismatch computation. IFAC- Pap. 55, 181–186. http://dx.doi.org/10.1016/j.ifacol.2022.09.092, arXiv:2201.04487.

Grandits, T., Verhülsdonk, J., Haase, G., Effland, A., Pezzuto, S., 2023. Digital twinning of cardiac electrophysiology models from the surface ECG: a geodesic backpropagation approach. IEEE Trans. Biomed. Eng. 1–8. http://dx.doi.org/10.1109/TBME.2023.3331876, arXiv:2308.08410.

Ijiri, T., Ashihara, T., Yamaguchi, T., Takayama, K., Igarashi, T., Shimada, T., Namba, T., Haraguchi, R., Nakazawa, K., 2008. A procedural method for modeling the purkinje fibers of the heart. J. Physiol. Sci. : JPS 58 (7), 481–486. http://dx.doi.org/10.2170/physiolsci.RP003208, URL http://www.ncbi.nlm.nih.gov/pubmed/18926006.

Jones, D.R., Schonlau, M., Welch, W.J., 1998. Efficient global optimization of expensive black-box functions. J. Global Optim. 13, 455–492.

Kahlmann, W., Poremba, E., Potyagaylo, D., Dössel, O., Loewe, A., 2017. Modelling of patient-specific purkinje activation based on measured ECGs. Curr. Dir. Biomed. Eng. 3 (2), 171–174.

Kong, F., Shadden, S.C., 2022. Learning whole heart mesh generation from patient images for computational simulations. IEEE Trans. Med. Imaging 42 (2), 533–545.

Kumar, P.S., Kumaraswamidhas, L., Laha, S., 2021. Selection of efficient degradation features for rolling element bearing prognosis using Gaussian Process Regression method. ISA Trans. 112, 386–401.

Lee, A.W., Costa, C.M., Strocchi, M., Rinaldi, C.A., Niederer, S.A., 2018. Computational modeling for cardiac resynchronization therapy. J. Cardiovasc. Transl. Res. 11, 92–108.

Lindenmayer, A., 1968. Mathematical models for cellular interactions in development, Part I & II. J. Theoret. Biol. 18 (3), 280–315.

Maffessanti, F., Jadczyk, T., Kurzelowski, R., Regoli, F., Caputo, M.L., Conte, G., Gołba, K.S., Biernat, J., Wilczek, J., Dabrowska, M., Pezzuto, S., Moccetti, T., Krause, R., Wojakowski, W., Prinzen, F.W., Auricchio, A., 2020. The influence of scar on the spatio-temporal relationship between electrical and mechanical activation in heart failure patients. EP Eur. 22 (5), 777–786. http://dx.doi.org/10.1093/europace/euz346.

Magat, J., Fouillet, A., Constantin, M., Haliot, K., Naulin, J., El Hamrani, D., Benoist, D., Charron, S., Walton, R., Bernus, O., et al., 2021. 3D magnetization transfer (MT) for the visualization of cardiac free-running Purkinje fibers: an ex vivo proof of concept. Magn. Reson. Mater. Phys. Biol. Med. 1–14.

Neic, A., Campos, F.O., Prassl, A.J., Niederer, S.A., Bishop, M.J., Vigmond, E.J., Plank, G., 2017. Efficient computation of electrograms and ECGs in human whole heart simulations using a reaction-eikonal model. J. Comput. Phys. 346, 191–211. http://dx.doi.org/10.1016/j.jcp.2017.06.020, URL http://www.sciencedirect.com/science/article/pii/S0021999117304655.

Palamara, S., Vergara, C., Catanzariti, D., Faggiano, E., Pangrazzi, C., Centonze, M., Nobile, F., Maines, M., Quarteroni, A., 2014. Computational generation of the Purkinje network driven by clinical measurements: the case of pathological propagations. Int. J. Numer. Methods Biomed. Eng. 30 (12), 1558–1577.

Pan, J., Tompkins, W.J., 1985. A real-time QRS detection algorithm. IEEE Trans. Biomed. Eng. (3), 230–236.

Pedregosa, F., Varoquaux, G., Gramfort, A., Michel, V., Thirion, B., Grisel, O., Blondel, M., Prettenhofer, P., Weiss, R., Dubourg, V., Vanderplas, J., Passos, A., Cournapeau, D., Brucher, M., Perrot, M., Duchesnay, E., 2011. Scikit-learn: Machine learning in python. J. Mach. Learn. Res. 12, 2825–2830.

Pezzuto, S., Kaľavský, P., Potse, M., Prinzen, F.W., Auricchio, A., Krause, R., 2017. Evaluation of a rapid anisotropic model for ECG simulation. Front. Physiol. 8, 265. http://dx.doi.org/10.3389/fphys.2017.00265.

Pezzuto, S., Perdikaris, P., Sahli Costabal, F., 2022. Learning cardiac activation maps from 12-lead ECG with multi-fidelity Bayesian optimization on manifolds. IFAC- Pap. 55, 175–180. http://dx.doi.org/10.1016/j.ifacol.2022.09.091, arXiv:2203.06222.

Pezzuto, S., Prinzen, F.W., Potse, M., Maffessanti, F., Regoli, F., Caputo, M.L., Conte, G., Krause, R., Auricchio, A., 2021. Reconstruction of three-dimensional biventricular activation based on the 12-lead electrocardiogram via patient-specific modelling. EP Eur. 23 (4), 640–647.

Potse, M., 2018. Scalable and accurate ECG simulation for reaction-diffusion models of the human heart. Front. Physiol. 9, 370.

Potse, M., Krause, D., Kroon, W., Murzilli, R., Muzzarelli, S., Regoli, F., Caiani, E., Prinzen, F.W., Krause, R., Auricchio, A., 2014. Patient-specific modelling of cardiac electrophysiology in heart-failure patients. Europace 16 (suppl_4), iv56–iv61.

Quaglino, A., Pezzuto, S., Koutsourelakis, P., Auricchio, A., Krause, R., 2018. Fast uncertainty quantification of activation sequences in patient-specific cardiac electrophysiology meeting clinical time constraints. Int. J. Numer. Methods Biomed. Eng. 34 (7), e2985.

Rasmussen, C.E., Williams, C.K.I., 2006. Gaussian Processes for Machine Learning. MIT Press, Cambridge.

Remacle, J.-F., Geuzaine, C., Compere, G., Marchandise, E., 2010. High-quality surface remeshing using harmonic maps. Internat. J. Numer. Methods Engrg. 83 (4), 403–425.

Robert, C., Casella, G., 2013. Monte Carlo Statistical Methods. Springer Science & Business Media.

Sahli Costabal, F., Hurtado, D., Kuhl, E., 2016. Generating Purkinje networks in the human heart. J. Biomech. 49, 2455–2465. http://dx.doi.org/10.1016/j.jbiomech.2015.12.025.

Sebastian, R., Zimmerman, V., Romero, D., Frangi, A.F., 2011. Construction of a computational anatomical model of the peripheral cardiac conduction system. IEEE Trans. Biomed. Eng. 58 (12 PART 2), 3479–3482. http://dx.doi.org/10.1109/TBME.2011.2166553.

Sebastian, R., Zimmerman, V., Romero, D., Sanchez-Quintana, D., Frangi, A.F., 2013. Characterization and modeling of the peripheral cardiac conduction system. IEEE Trans. Med. Imaging 32 (1), 45–55. http://dx.doi.org/10.1109/TMI.2012.2221474, URL http://www.ncbi.nlm.nih.gov/pubmed/23047864.

Sunnåker, M., Busetto, A.G., Numminen, E., Corander, J., Foll, M., Dessimoz, C., 2013. Approximate bayesian computation. PLoS Comput. Biol. 9 (1), e1002803.

Tawara, S., 1906. Das reizleitungssystem des Säugetierherzens. Fischer.

ten Tusscher, K., Noble, D., Noble, P., Panfilov, A., 2004. A model for human ventricular tissue. Am. J. Physiol – Hear. Circ. Physiol. 286 (4), H1573–89. http://dx.doi.org/10.1152/ajpheart.00794.2003, URL http://www.ncbi.nlm.nih.gov/pubmed/14656705.

Tsao, C.W., Aday, A.W., Almarzooq, Z.I., Anderson, C.A., Arora, P., Avery, C.L., Baker-Smith, C.M., Beaton, A.Z., Boehme, A.K., Buxton, A.E., et al., 2023. Heart disease and stroke statistics—2023 update: a report from the American heart association. Circulation 147 (8), e93–e621.

Vergara, C., Lange, M., Palamara, S., Lassila, T., Frangi, A.F., Quarteroni, A., 2016. A coupled 3D–1D numerical monodomain solver for cardiac electrical activation in the myocardium with detailed purkinje network. J. Comput. Phys. 308, 218–238.

Vergara, C., Palamara, S., Catanzariti, D., Nobile, F., Faggiano, E., Pangrazzi, C., Centonze, M., Maines, M., Quarteroni, A., Vergara, G., 2014. Patient-specific generation of the Purkinje network driven by clinical measurements of a normal propagation. Med. Biol. Eng. Comput. 813–826. http://dx.doi.org/10.1007/s11517-014-1183-5.

Verzaal, N.J., van Deursen, C.J., Pezzuto, S., Wecke, L., van Everdingen, W.M., Vernooy, K., Delhaas, T., Auricchio, A., Prinzen, F.W., 2022. Synchronization of repolarization after cardiac resynchronization therapy: A combined clinical and modeling study. J. Cardiovasc. Electrophysiol. 33 (8), 1837–1846.

Vigmond, E.J., Stuyvers, B.D., 2016. Modeling our understanding of the His-Purkinje system. Prog. Biophys. Mol. Biol. 120 (1–3), 179–188.

Vijayaraman, P., Pokharel, P., Subzposh, F.A., Oren, J.W., Storm, R.H., Batul, S.A., Beer, D.A., Hughes, G., Leri, G., Manganiello, M., et al., 2023. His-Purkinje conduction system pacing optimized trial of cardiac resynchronization therapy (HOT-crt) versus biventricular pacing. JACC: Clin. Electrophysiol..

Virtanen, P., Gommers, R., Oliphant, T.E., Haberland, M., Reddy, T., Cournapeau, D., Burovski, E., Peterson, P., Weckesser, W., Bright, J., van der Walt, S.J., Brett, M., Wilson, J., Millman, K.J., Mayorov, N., Nelson, A.R.J., Jones, E., Kern, R., Larson, E., Carey, C.J., Polat, İ., Feng, Y., Moore, E.W., VanderPlas, J., Laxalde, D., Perktold, J., Cimrman, R., Henriksen, I., Quintero, E.A., Harris, C.R., Archibald, A.M., Ribeiro, A.H., Pedregosa, F., van Mulbregt, P., SciPy 1.0 Contributors, 2020. SciPy 1.0: Fundamental algorithms for scientific computing in python. Nature Methods 17, 261–272. http://dx.doi.org/10.1038/s41592-019-0686-2.